Non-canonical Wnt/PCP signalling regulates intestinal stem cell lineage priming towards enteroendocrine and Paneth cell fates

Anika Böttcher[1,2,3], Maren Büttner[4], Sophie Tritschler[4,5], Michael Sterr[1,2,3], Alexandra Aliluev[1,2,3], Lena Oppenländer[1,2,3], Ingo Burtscher[1,2,3], Steffen Sass[4], Martin Irmler[3,6], Johannes Beckers[3,6,7], Christoph Ziegenhain[8], Wolfgang Enard[8], Andrea C. Schamberger[9], Fien M. Verhamme[9], Oliver Eickelberg[9], Fabian J. Theis[4,10#], and Heiko Lickert[1,2,3,10,11#]

[1]Institute of Diabetes and Regeneration Research, Helmholtz Diabetes Center**,** Helmholtz Center Munich, 85764 Neuherberg, Germany.

[2]Institute of Stem cell Research**,** Helmholtz Center Munich, 85764 Neuherberg, Germany.

[3]German Center for Diabetes Research (DZD), 85764 Neuherberg, Germany.

[4]Institute of Computational Biology, Helmholtz Center Munich, 85764 Neuherberg, Germany.

[5]School of Life Sciences Weihenstephan, Technical University of Munich, Freising, Germany

[6]Institute of Experimental Genetics, Helmholtz Center Munich, 85764 Neuherberg, Germany.

[7]Technical University of Munich, Chair of Experimental Genetics, 85354 Freising, Germany.

[8]Department Biology II, Anthropology and Human Genomics, Ludwig-Maximilians-University of Munich, 82152 Martinsried, Germany.

[9]Comprehensive Pneumology Center, Helmholtz Center Munich, 81377 Munich, Germany.

[10]Technical University of Munich, 80333 Munich, Germany.

[11]Lead contact

[#]Authors for correspondence: Heiko Lickert (heiko.lickert@helmholtz-muenchen.de) and Fabian J. Theis (fabian.theis@helmholtz-muenchen.de)

Correspondence and requests for materials should be addressed to H.L. (heiko.lickert@helmholtz-muenchen.de)

Heiko Lickert, Helmholtz Center Munich, Ingolstaedter Landstraße 1, 85764, Neuherberg, Germany. Phone: +49 89 31873760, FAX: +49 89 31873761

Abstract

A detailed understanding of intestinal stem cell (ISC) self-renewal and differentiation is required to treat chronic intestinal diseases. However, different models of ISC lineage hierarchy[1–6] and segregation[7–12] are debated. Here we discovered Wnt/planar cell polarity (PCP)-activated ISCs that are primed towards the enteroendocrine or Paneth cell lineage. Strikingly, integration of time-resolved lineage labelling with single-cell gene expression analysis revealed that both lineages are directly recruited from ISCs via unipotent transition states, challenging the existence of formerly predicted bi- or multipotent secretory progenitors[7–12]. Transitory cells that mature into Paneth cells are quiescent and express both stem cell and secretory lineage genes, indicating that these cells are the previously described $Lgr5^+$ label-retaining cells[7]. Finally, Wnt/PCP-activated $Lgr5^+$ ISCs are molecular indistinguishable from Wnt/β-catenin-activated $Lgr5^+$ ISCs, suggesting that lineage priming and cell-cycle exit is triggered at the post-transcriptional level by polarity cues and a switch from canonical to non-canonical Wnt/PCP signalling. Taken together, we redefine the mechanisms underlying ISC lineage hierarchy and identified the Wnt/PCP pathway as a new niche signal preceding lateral inhibition in ISC lineage priming and segregation.

Main

The intestinal epithelium renews continuously throughout life from a pool of Wnt/β-catenin-dependent Lgr5^{+} intestinal stem cells (ISCs)[1,13]. Lineage commitment of Lgr5^{+} ISCs has been viewed as a binary decision between an absorptive and a secretory progenitor through Notch/Delta-mediated lateral inhibition[14,15]. However, controversies exist regarding the potency of secretory progenitors and their differentiation routes into goblet cells, tuft cells, Paneth cells (PCs) or enteroendocrine cells (EECs)[7–12]. One possibility is that ISCs are functionally heterogeneous and directly differentiate into secretory cell types without passing through proposed stages of bi- or multipotent secretory progenitors. Indeed, functional heterogeneity of ISCs is evident in that i) ISCs positioned at the centre and the periphery of the crypt base produce different clone sizes[16], ii) reserve stem cells are described at crypt position +4[17–20] and iii) not all Lgr5^{+} cells constitute functional ISCs *in vivo*[21] and some might correspond to non-cycling Lgr5^{+} label-retaining cells (LRCs), which are PC and/or EEC progenitors[7]. The non-canonical Wnt/planar cell polarity (PCP) pathway controls beta cell differentiation in the pancreas[22,23] and determines functional heterogeneity in the islets of Langerhans[23,24]. Remarkably, the canonical Wnt/β-catenin pathway (which is required for the maintenance of Lgr5^{+} ISCs) and the non-canonical Wnt/PCP pathway share signalling components and antagonize each other's function in some tissues[25,26]. Hence, Wnt/PCP signalling is a prime candidate pathway to control ISC heterogeneity and lineage choice.

To analyse the impact of Wnt/PCP activation on ISC self-renewal and differentiation in the crypt stem cell niche we took advantage of the first reported sentinel for pathway activation, our knock-in *Flattop* (*Fltp*)^{ZV} (Lac<u>Z</u> and H2B-<u>V</u>enus) dual reporter mouse model (Fig. 1a)[23,27]. In this mouse model, *Fltp*-H2B Venus reporter (FVR) activity is cell-cycle dependent and restricted to quiescent and terminally differentiated cells that had previously induced *Fltp* expression during Wnt/PCP acquisition[23,27]. When analysing small intestinal (SI) crypt cells in this model, we could distinguish three populations based on their FVR label intensity: FVR^{neg}, FVR^{low} and FVR^{hi} cells (Fig. 1b). We isolated these populations using flow cytometry and characterized them using genome-wide transcriptional profiling (Fig. 1c and Extended Data Fig. 1a, b). KEGG pathway analysis revealed that the FVR^{neg}, FVR^{low} and FVR^{hi} populations can be distinguished

by their expression of genes involved in absorption, hormone secretion and immune-regulation, respectively, and by genes regulating cell-cycle behaviour and metabolic activity (Extended Data Fig. 1c and Supplementary Table 1). FVR^{low} and FVR^{hi} cells were highly enriched in transcripts associated with different EEC subsets (*Chga*, *Chgb*, *Nkx2-2*, *Neurod1*) and the PC lineage (*Nupr1*, *Dll4*, *Mmp7*, *Lyz1*), respectively, when compared to $Lgr5^{high}$ ISCs (Fig. 1c and Extended Data Fig. 1d, e). Further, the FVR^{hi} population co-expressed ISC markers (Fig. 1c). This combined expression pattern is similar to the transcriptional profile of quiescent $Lgr5^{+}$ LRCs (Fig. 1c)[7]. The low expression of cell proliferation genes (*Ccnd1*, *Ki67*) and the high level of the cell-cycle inhibitor gene *Cdkn1a* in both FVR^{+} populations suggested that FVR^{+} cells undergo terminal differentiation (Extended Data Fig. 1f). Indeed, FVR activity labelled a subset of the postmitotic secretory lineage namely essentially all $Lyz1^{+}$ PCs (95.58%) and $ChgA^{+}$ crypt EECs (96.13%), but not goblet or tuft cells (Fig. 1d-f and Extended Data Fig. 1g-i). Using a targeted single-cell qRT-PCR approach, we found that *Fltp* expression was restricted to a few FVR^{low} EECs and FVR^{hi} PCs, and to a subset of $Lgr5^{+}$ ISCs (6.2%) (Fig. 1g). *Fltp* mRNA expression was induced by Wnt/PCP ligand stimulation indicating that Fltp is also a Wnt/PCP effector in the gut (Fig. 1h). From these data we conclude that i) *Fltp* is transiently expressed in ISCs, and ii) FVR due to reporter protein stability labels the immediate daughter cells of $Fltp^{+}$ ISCs; i.e., more than 95% of the EECs and PCs.

Homogeneity and equipotency of the ISC pool is vividly discussed[3–5,16–21,28,29]. Our data suggested that $Fltp^{+}$ ISCs are primed towards the EEC and/or PC lineage. To determine the mechanism underlying ISC heterogeneity and lineage priming, we next used a dual-fluorescent Cre-reporter $Fltp^{T2AiCre/+}$; $Gt(ROSA)26^{mTmG/+}$ mouse line (Extended Data Fig. 2a)[30,31]. In this model, Cre recombinase induces a switch from membrane-Tomato (mT) to membrane-GFP (mG). The intermediate mTmG state can be captured by flow cytometry and highly expresses *Fltp* (Fig. 2a-c). *In vivo*, $Fltp^{+}$ mTmG cells predominantly located at crypt position +4/+5 (Fig. 2d, e). Consistent with the transient expression of the Wnt/PCP reporter gene *Fltp* in a subset of $Lgr5^{+}$ ISCs (Fig. 1g), the Wnt/PCP activated $Fltp^{+}$ mTmG cells and Wnt/β-catenin activated $Lgr5^{+}$ ISCs are closely related as exemplified by similar expression of the $Lgr5^{+}$ ISC signature genes[29], lineage-specifying genes and Notch pathway genes, as well as the lack of $Lgr5^{+}$ LRC

markers[7] (Fig. 2f-i and Extended Data Fig. 2b, c). However, we found that less mTmG cells were in cell-cycle and formed organoids compared to Lgr5$^+$ ISCs (Extended Data Fig. 2d-i). As *Fltp*$^+$ mTmG cells possessed limited self-renewal capacity *in vitro* we next analysed whether chemical injury of the intestine can activate these cells. In contrast to Wnt/β-catenin activated Lgr5$^+$ ISCs, mTmG cells were resistant to 5-FU treatment but showed reduced mitotic activity (Extended Data Fig. 3a-i). We sporadically detected lineage-traced villi in the small intestine in homeostasis and the number did not increase in 5-FU treated mice indicating that mTmG cells do not contribute to regeneration after intestinal injury (Extended Data Fig. 3j-l). Together, these data show that Fltp$^+$ ISCs are transcriptionally similar to Lgr5$^+$ ISCs but possess limited self-renewal capacity *in vitro* and *in vivo*. Further, we conclude that Wnt/PCP signalling-induced lineage priming in Fltp$^+$ ISCs represents the earliest step in the commitment of ISCs towards the PC or EEC lineage. These early cell fate decisions are triggered at the post-transcriptional level by polarity cues and precede Notch/Delta-mediated lateral inhibition.

Secretory lineage specification and in particular the signalling pathways that regulate secretory subtype specification remain poorly understood[7–12] (Extended Data Fig. 4a, b). Our data suggested that the PC and EEC lineage directly allocate from ISCs. To elucidate the lineage hierarchy and conclude on lineage relationships in the intestinal epithelium, we made use of the *Fltp*^{ZV} and Foxa2 Venus Fusion (FVF) reporter mouse lines[27,32] that label rare intestinal cell populations and performed single-cell RNA sequencing (scRNAseq) of 60,000 cells in homeostasis (Fig. 3a). Using this approach, we could highly enrich for the PC, EEC, goblet and tuft cell lineages (Fig. 3b, c, Extended Data Fig. 4c, d). Due to the enrichment and high resolution of the secretory lineages we could identify all described intestinal epithelial populations and in addition lineage-specified progenitors with proliferative activity and distinct expression profiles (Fig. 3b-e, Extended Data Fig. 4c-g, Extended Data Fig. 5a-c, Supplementary Table 2). Further, to computational reconstruct possible lineage relationships and differentiation trajectories we used partitioned graph abstraction (PAGA)[33]. Strikingly, we found that all lineages originated from ISCs. Progenitor states were highly interconnected reflecting the high plasticity of intestinal epithelial cells[34] (Extended Data Fig. 5d). Together, these data imply that for each intestinal lineage a progenitor with a distinct transcriptional signature exists and that all lineages directly allocate from ISCs.

As transcriptomes alone may not accurately determine the future cell fate of ISCs and progenitors[35,36] we combined temporal-resolved lineage labelling with a highly sensitive single-cell qRT-PCR approach to fine-map fate decisions towards the PC and EEC lineage (Fig. 4a, b). We determined the expression of 80 well-known and functionally important intestinal signature genes (Fig. 4b and Supplementary Table 3). To gain temporal and progenitor state resolution we included: i) Lgr5^{hi} ISCs from *Lgr5-ki* mice, ii) early and late mTmG cells from *Fltp*$^{T2AiCre/+}$; *Gt(ROSA)26*$^{mTmG/+}$ mice, iii) FVR^{+}/Lgr5^{hi} and FVR^{+}/Lgr5^{low} double-positive cells from *Fltp*^{ZV}/*Lgr5-ki* dual reporter mice (Fig. 4c-e), and iv) Neurog3-expressing EEC progenitors from Ngn3-Venus reporter mice[37]. UMAP visualization of the single-cell qRT-PCR data showed that the flow-sorted FVR^{hi} PCs grouped into one defined cluster, whereas the FVR^{low} EECs grouped into two clusters (Fig. 4f). Early mTmG cells grouped together with Lgr5^{hi} ISCs and late mTmG cells grouped together with a subset of FVR^{low} cells (Fig. 4f).

To delineate the ISC differentiation path into the EEC and PC lineages we used PAGA[33]. Ordering of cells along a pseudotime as a proxy for real-time differentiation identified three terminal states from our single-cell qRT-PCR snapshot data: the PC branch with terminal state 1, the EEC branch with terminal state 2 and a third branch with unassigned cells (Fig. 4g-j and Extended Data Fig. 6a). Separation into the EEC and PC lineages occurred early and still within the ISC population, which reinforces that EECs and PCs directly allocate from Lgr5^{+} ISCs (Fig. 4i, j and Extended Data Fig. 6b). Plotting gene expression versus pseudotime revealed that cells differentiate via lineage-specific unipotent transition states characterized by downregulation of stem cell markers for the EEC branch and co-expression of stem-cell and secretory markers for the PC branch (Extended Data Fig. 6b-f). Unassigned cells were mainly late mTmG and FVR^{low} cells (Fig. 4j) and did not express mature EEC or PC markers (Extended Data Fig. 6a, b. Together, the pseudotemporal analysis further supports our real-time lineage reporter-based finding that PCs and EECs directly allocate from ISCs via unipotent progenitors.

Single-cell transcriptomics data suggested that PCs are mainly formed via a PC/goblet cell precursor and that only a small subset directly differentiates from ISCs[2]. However, our integrated analysis of lineage labelling with single-cell gene expression indicates that in addition to EECs

most of the PCs also directly allocate from ISCs via a unipotent transition state comprising mainly $Lgr5^{+}/FVR^{+}$ double-positive cells (Fig. 4j and Extended Data Fig. 6).

Using the FVR mice we obtained transcriptional profiles of more than 20,000 cells from the rare and difficult to capture PC lineage[28] (Fig. 3). When we investigated the transition of ISCs to PCs we identified a ISC population that connects to the PC progenitor population, which we termed PC-primed ISCs (Fig. 5a). In addition, we found two mature PC types which differ in the expression of *Lyz2* (Fig. 5b). Pseudotemporal ordering of ISCs and PC subclusters placed the PC progenitor in between the mature PCs and ISCs, while PC-primed ISCs link to PC progenitors (Fig. 5c). The co-expression of stem-cell and secretory lineages genes in the PC progenitor suggested that these are the recently described quiescent $Lgr5^{+}$ LRCs[7] (Fig. 4, 5c, d and Extended Data Fig. 6a-c). Quiescent or slowly cycling intestinal cells persist for more than 10 days and thus are defined by the property of label-retention. Differentiated intestinal lineages are renewed every 4-5 days with the exception of PCs that have a lifespan of about 6-8 weeks. To assess label-retention within the FVR^{+} population we "birth-dated" this population with 5-bromodeoxyuridine (BrdU) (Fig. 5e-g). After a chase period of 10 days, 30% of the FVR^{+} cells retained the label and were non-PCs ($Lyz1^{-}$), and hence LRCs (Fig. 5h). After a chase period of 21 days, all $BrdU^{+}$ LRCs present in the crypt were also FVR^{+}. An increase in $FVR^{+}/BrdU^{+}/Lyz1^{+}$ cells implied that FVR^{+} LRCs give rise to PCs (Fig. 5h). Like $Fltp^{+}$ ISCs, FVR^{+} LRCs were predominantly located at position +4/+5 (Fig. 2d, e and Fig. 5i-k). These results indicate that PCs directly arise from ISCs via a quiescent, label-retaining transition state, which is characterized by co-expression of stem cell and secretory lineage markers. The identification of lineage-specific unipotent transition states together with the fact that FVR labels more than 95% of all PCs and EECs, but not goblet or tuft cells challenges the existence of formerly predicted bi- or multipotent secretory progenitors.

Fltp is transiently expressed in ISCs that acquired Wnt/PCP activation and are committed to differentiate into PCs and EECs (Fig. 1g, Fig. 2f, g). Cell ordering along the pseudotime confirmed that i) Wnt/PCP signalling is specifically activated in ISCs that differentiate towards PCs and EECs indicated by upregulation of several Wnt/PCP genes such as *Vangl2*, *Dvl2*, *Ror2* and *Celsr1* and ii) Wnt/PCP pathway activation precedes Notch/Delta-mediated lateral inhibition and cell-cycle exit (Extended Data Fig. 7a, b and Extended Data Fig. 2b). Consistent with the

198 expression of core pathway components we also detected increased expression of Wnt/PCP
199 pathway genes and Jnk activity in the FVR^{+} population, indicative of active Wnt/PCP signalling
200 (Extended Data Fig. 7c-f). To further corroborate a role of Wnt/PCP signalling in cell fate
201 regulation we analysed $Celsr1^{crsh/+}$; $Fltp^{ZV/ZV}$ double mutant mice. The protocadherin Celsr1 is a
202 core Wnt/PCP component and member of a family consisting of Celsr1-3. The Crash (Crsh)
203 mutant has been identified in an ENU mutagenesis screen[38]. Homozygous and heterozygous
204 $Celsr1^{crsh}$ mutant mice show the classical Wnt/PCP phenotype including neural tube closure
205 defects and disruption of planar polarity of inner ear hair cells[38]. The missense mutation in the
206 *Celsr1* gene results in a reduction of *Celsr1* mRNA expression to 50% in crypt cells from
207 heterozygous $Celsr1^{crsh/+}$; $Fltp^{ZV/+}$ compound mutant mice (Extended Data Fig. 8a). Gene
208 expression analysis of 14,000 mutant cells (from *n=4* mutant mice) revealed that the PC
209 progenitor population is less proliferative and aberrant gene expression of known secretory
210 lineage regulators (e.g. *Sox9*, *Atoh1*, *Spdef*, *Foxa3*, *Tead2* and *Jun*) and potentially new
211 regulators (e.g. *Ybx1*, *Pa2g4*, *Hnrnpk*) as well as canonical Wnt target genes specifically in the
212 PC lineage suggesting disturbances in the differentiation of PCs (Extended Data Fig. 8b-f).
213 Assessment of PC and EEC numbers showed a slight reduction of PCs when compared to control
214 mice (Extended Data Fig. 8g-i). These weak disturbances in gene expression and PC and EEC
215 numbers in this mutant mouse model is most likely due to functional redundancy of Wnt/PCP
216 proteins during PC and EEC differentiation (Extended Data Fig. 7).

217 Taken together, we identified the Wnt/PCP pathway as a new niche signal that determines stem
218 cell fate. We propose that a switch from Wnt/β-catenin to non-canonical Wnt/PCP signalling
219 induces PC and EEC lineage priming and cell-cycle exit of ISCs. This is consistent with our
220 recent findings that Wnt/PCP activation triggers functional maturation and cell-cycle exit of
221 endocrine insulin-producing β-cells in the pancreatic islet[23] and suggests that polarity cues
222 regulate cell heterogeneity and terminal differentiation in the crypt and islet cell niche.

223

224

Figure legends

Fig. 1: FVR labels the secretory enteroendocrine and Paneth cell lineages.

a, Schematic of the *Fltp* loss-of-function and NLS-LacZ/H2B-Venus transcriptional reporter allele *(Fltp^{ZV})*.

b, Laser scanning confocal microscopy (LSM) image of a representative small intestinal (SI) crypt isolated from an adult *Fltp$^{ZV/+}$* reporter mouse depicting FVR$^{hi/low/neg}$ crypt cells. FVR (Venus, green), DAPI (blue, nuclei), E-cadherin (E-cad, red, membrane). Image representative of 4 mice. Scale bars, 25 μm.

c, Experimental design for microarray analysis of the three small intestinal (SI) crypt cell populations distinguishable by FVR activity. The heatmap depicts the expression profiles of key stem-cell and intestinal lineage genes. Expression is scaled row-wise and the colours range from dark blue (low expression) to orange (high expression) and represent normalized expression (row z-score). ISC, intestinal stem cell. CBC, crypt base columnar cell. Sec. progenitor, secretory progenitor. EEC, enteroendocrine cell.

d, LSM images showing FVR (Venus, green) expression in the secretory lineages in the intestine of adult *Fltp$^{ZV/+}$* mice co-stained against ChgA (red, enteroendocrine cells), Lyz1 (white, Paneth cells), Muc2 (red, goblet cells), and Dclk1 (red, tuft cells). DAPI (blue) stains the nucleus. 4 independent experiments with one mouse per experiment. Scale bars, 75 μm.

e, f, LSM image depicting a representative SI crypt isolated from adult *Fltp$^{ZV/+}$* reporter mice with indicated FVR$^{neg/low/hi}$ cells stained for DAPI (blue, nucleus), FVR (Venus, green), ChgA (red, enteroendocrine cells), and Lyz1 (white, Paneth cells) (**e**) and quantification of Lyz1^{+} FVR^{+} Paneth cells (PCs) and ChgA^{+} FVR^{+} enteroendocrine cells (EECs) (**f**). For PCs: n = 7 mice with 99 analysed crypts. For EECs: n = 5 mice with 76 analysed crypts. Data are presented as mean values +/- SD. Scale bar, 25 μm.

g, Relative abundance of *Fltp^{+}* Lgr5^{hi}, FVR^{low} and FVR^{hi} cells determined by single-cell qRT-PCR. n = 145 Lgr5^{hi} cells from 3 Lgr5-ki mice; n = 112 FVR^{low} cells and n = 126 FVR^{hi} cells from 3 Fltp$^{ZV/+}$ mice.

h, *Fltp* expression in crypts treated with indicated Wnt/PCP ligands for two days. n = 4 independent experiments. Data are presented as mean values +/- SEM. Two-tailed Student's *t*-test.

Fig. 2: Wnt/β-catenin and non-canonical Wnt/PCP activated Lgr5^{+} ISCs are indistinguishable at the transcriptional level.

a, b, Flow cytometry analysis (**a**) and relative abundance (**b**) of Fltp lineage^{-} (mT), Fltp^{+} intermediate cells (mTmG) and Fltp lineage^{+} (mG) crypt cells isolated from *Fltp*$^{T2AiCre/+}$;*Gt(ROSA)26*$^{mTmG/+}$ mice. n = 6 mice. Data are presented as mean values +/- SEM.

c, qRT-PCR data comparing relative *Fltp* expression in mTmG crypt cells isolated from *Fltp*$^{T2AiCre/+}$;*Gt(ROSA)26*$^{mTmG/+}$ mice and Lgr5^{hi} ISCs isolated from Lgr5-ki mice. n = 3 experiments with a total of 3 mice [Au: is this correct? How many mice?] for Lgr5^{hi} cells. n = 2 experiments with a total of 4 mice for mTmG cells.

d, e, Representative LSM images of *Fltp*$^{+}$ intermediate mTmG cells at indicated positions. SI crypts from *Fltp*$^{T2AiCre/+}$;*Gt(ROSA)26*$^{mTmG/+}$ mice were stained for DAPI (blue, nucleus), mT (red, RFP), mG (green, GFP), and Lyz1 (white, Paneth cells). Scale bars, 25 μm. (**d**). Abundance of mTmG cells at indicated positions (**e**). n = 3 mice.

f, g, Representative LSM images of Lgr5^{hi} and mTmG cells isolated by flow cytometry and stained for active, phosphorylated Jun N-terminal kinase (pJnk, white) indicating active Wnt/PCP signalling and DAPI (blue, stains nuclei) (**f**). Quantification of the mean fluorescent intensity of pJnk (**g**). n = 3 mice for Lgr5^{hi} cells. n = 5 mice for mTmG cells. Data are presented as mean values +/- SD. Two-tailed Student's *t*-test. Scale bars, 50 μm.

h, MA-plot comparing the expression of ISC signature genes in mTmG and Lgr5^{hi} (ISCs) cells. Differentially expressed genes (FDR < 0.01) are indicated in red. The y-axis indicates the fold change in log2 and the x-axis indicates the mean log2 expression value. *Clca1* is the only significantly regulated gene. n = 6 mice for Lgr5^{hi}. n = 4 mice for mTmG.

i, MA-plot comparing the expression of lineage-specifying genes in mTmG and Lgr5^{hi} cells. The y-axis indicates the fold change in log2 and the x-axis indicates the mean log2 expression value. No gene is significantly regulated. $n = 6$ mice for Lgr5^{hi}. $n = 4$ mice for mTmG.

Fig. 3: Subtype enrichment of crypt cells reveals distinct progenitor states for all intestinal lineages.

a, Experimental overview. SI crypt cells were obtained from wild-type and reporter (*Fltp*$^{ZV/+}$, Foxa2$^{FVF/FVF}$) mice. FACS was used to enrich rare crypt cell populations from reporter mice. Transcriptional profiling of single cells was performed using the 10X Genomics platform.

b, Reporter mice enable the identification of rare cell states. Cell-density plots of FVR and FVF based enrichment compared to a non-enriched sample. No enrichment (pooled cells from two mice), 50% FVR enrichment (pooled cells from two mice, flow-enriched FVR^{+} cells were mixed with non-enriched cells in a ratio of 1:2), 90% FVR enrichment (pooled cells from two mice, flow-enriched FVR^{+} cells were mixed with non-enriched cells in a ratio of 9:1), 50% FVF enrichment (pooled cells from three mice, flow-enriched FVF^{+} cells were mixed with non-enriched cells in a ratio of 1:2).

c, Bar plot depicting the relative abundance of progenitor and mature cell types in the non-enriched, and FVR- and FVF-enriched sample. FVR enrichment enables the isolation of rare PC progenitors and mature PCs whereas FVF enrichment allows the efficient extraction of the EEC and goblet cell lineage compared to the non-enriched sample. ISC, intestinal stem cell. EC pro, enterocyte progenitor. EC, enterocyte. GC pro, goblet cell progenitor. Early GC, early goblet cell. GC, mature goblet cell. PC pro, Paneth cell progenitor. PC, Paneth cell. EEC pro, enteroendocrine cell progenitor. EEC, enteroendocrine cell. TC pro, tuft cell progenitor. TC, tuft cell.

d, UMAP plot of all control intestinal crypt cells highlighting progenitor cell-type annotation. Grey lines depict 30 nearest neighbors for each cell. Cells were obtained from 10 samples including wild-type (control) and reporter mice for lineage enrichment.

e, The bar plot depicts the number of captured cells per cell type.

Fig. 4: Temporal-resolved lineage labelling and pseudotemporal ordering of intestinal crypt cells shows that EECs and PCs directly allocate from ISCs via unipotent transition states.

a, b, Schematic depicting the working hypothesis that non-canonical Wnt/PCP activated *Fltp*$^{+}$ ISCs are committed to differentiate into Paneth cells (PCs) and enteroendocrine cells (EECs) (**a**). Integration of lineage labelling and single-cell gene expression to elucidate the differentiation trajectories from ISCs into the Paneth and enteroendocrine lineage by single-cell qRT-PCR analysis of 80 genes from defined categories in Lgr5^{hi} ISCs, mTmG cells, FVR cells, FVR^{+}/Lgr5^{+} cells and Ngn3-VR cells (**b**).

c, d, FACS plot of crypt cells from *Fltp*$^{ZV/+}$; *Lgr5-ki* dual reporter mice depicting the separation of rare FVR^{+}/Lgr5^{+} (FVR^{+}/Lgr5^{hi}, FVR^{+}/Lgr5^{low}) cells from Lgr5^{+}-GFP and FVR single positive, and Lgr5-GFP and FVR negative cells (**c**) and quantification of FACS analysis (**d**). 0.5% of the crypt cells are FVR^{+}Lgr5^{+} double positive. *n* = 7 mice. Data are presented as mean values +/- SEM.

e, LSM live image of a representative SI crypt, cultured in matrigel, isolated from *Fltp*$^{ZV/+}$; Lgr5-ki mice showing rare FVR^{+} (red), Lgr5^{+} (green) double positive cells (arrowhead) located at position +4 (= supra-Paneth cell position). PC, Paneth cell. ISC, intestinal stem cell (Lgr5^{+}). Image representative of 3 mice. Scale bar, 10 µm.

f, g, h, UMAP projections of Lgr5^{hi} cells, early and late mTmG cells, FVR^{+}/Lgr5^{+} cells, FVR^{+} cells and Ngn3-VF endocrine progenitors based on the expression of 80 marker genes. Each dot represents a single cell. Colours indicate FACS groups (**f**), pseudotime computed using dpt (**g**), and cell-type clusters annotated based on marker genes (**h**).

i, PAGA plot showing relationship of cell type clusters from (h).

j, The bar plot depicts the contribution of FACS groups to stages in the PC and EEC branch.

Fig. 5: FVR marks Lgr5^{+} label-retaining cells that give rise to Paneth cells.

a, UMAP plot depicting the identified cell states during differentiation of ISCs towards PCs.

b, Dot plot showing the expression of selected genes.

c, Smoothed gene expression heatmap of differentially expressed genes of the displayed cell states plotted along diffusion pseudotime from ISCs to PCs.

d, ISC and PC score along pseudotime.

e, Experimental scheme of the 5-bromo-2'-deoxyuridine (BrdU) pulse-chase experiment. To assess label-retention, *Fltp*$^{ZV/+}$ mice were treated with BrdU for 14 days (d) and analysed after 10 and 21d.

f, Representative LSM images of duodenal sections stained for FVR (Venus, green), BrdU incorporation (red) and Lyz1 (white, Paneth cells) after 14d BrdU administration. Images representative of 4 mice. Scale bars, 25µm.

g, Relative proportion of FVR$^+$/BrdU$^+$ cells of total FVR$^+$ cells at the indicated time points. 14d BrdU: n = 4 mice with 1432 analysed FVR$^+$ cells; 10d chase: n = 2 mice with 785 analysed FVR$^+$ cells; 21d chase: n = 4 mice with 2401 analysed FVR$^+$ cells.

h, Relative abundance of Lyz1$^-$ (LRC) cells of total FVR$^+$/BrdU$^+$ cells at the indicated time points. 14d BrdU: n = 4 mice with 1432 analysed FVR$^+$ cells; 10d chase: n = 2 mice with 785 analysed FVR$^+$ cells; 21d chase: n = 4 mice with 2401 analysed FVR$^+$ cells.

i, j, k, Scheme depicting the compartmentalization of the SI crypt. Cycling ISCs (Lgr5$^+$) and PCs reside in the PC zone. Quiescent cells/LRCs locate at position +4/+5. The transit-amplifying zone (TA zone) contains mainly proliferative progenitors (**i**). Representative LSM images from duodenal sections stained for FVR (Venus, green), BrdU incorporation (red) and Lyz1 (white, Paneth cells) after 10d and 21d chase. The position (arrowhead) of the FVR$^+$ LRC (BrdU$^+$/Lyz1$^-$) is defined according to the scheme in (**i**). Quantification of FVR$^+$ LRCs (BrdU$^+$/Lyz1$^-$) at indicated positions (according to j). 14d BrdU: n = 116 cells (from 4 mice), 10d chase: n = 32 cells (from 2 mice), 21d chase: n = 55 cells (from 4 mice) (**k**). Scale bars, 25 µm (**j**).

References

1. Barker, N. *et al.* Identification of stem cells in small intestine and colon by marker gene Lgr5. *Nature* (2007) doi:10.1038/nature06196.

2. Grün, D. *et al.* De Novo Prediction of Stem Cell Identity using Single-Cell Transcriptome Data. *Cell Stem Cell* (2016) doi:10.1016/j.stem.2016.05.010.

3. Li, N., Nakauka-Ddamba, A., Tobias, J., Jensen, S. T. & Lengner, C. J. Mouse Label-Retaining Cells Are Molecularly and Functionally Distinct From Reserve Intestinal Stem Cells. *Gastroenterology* (2016) doi:10.1053/j.gastro.2016.04.049.

4. Li, N. *et al.* Single-cell analysis of proxy reporter allele-marked epithelial cells establishes intestinal stem cell hierarchy. *Stem Cell Reports* (2014) doi:10.1016/j.stemcr.2014.09.011.

5. Kim, T. H. *et al.* Single-Cell Transcript Profiles Reveal Multilineage Priming in Early Progenitors Derived from Lgr5+ Intestinal Stem Cells. *Cell Rep.* (2016) doi:10.1016/j.celrep.2016.07.056.

6. Potten, C. S. Stem cells in gastrointestinal epithelium: Numbers, characteristics and death. *Philos. Trans. R. Soc. B Biol. Sci.* (1998) doi:10.1098/rstb.1998.0246.

7. Buczacki, S. J. A. *et al.* Intestinal label-retaining cells are secretory precursors expressing lgr5. *Nature* (2013) doi:10.1038/nature11965.

8. Grün, D. *et al.* Single-cell messenger RNA sequencing reveals rare intestinal cell types. *Nature* (2015) doi:10.1038/nature14966.

9. Heuberger, J. *et al.* Shp2/MAPK signaling controls goblet/paneth cell fate decisions in the intestine. *Proc. Natl. Acad. Sci. U. S. A.* (2014) doi:10.1073/pnas.1309342111.

10. Shroyer, N. F., Wallis, D., Venken, K. J. T., Bellen, H. J. & Zoghbi, H. Y. Gfi1 functions downstream of Math1 to control intestinal secretory cell subtype allocation and differentiation. *Genes Dev.* (2005) doi:10.1101/gad.1353905.

11. van Es, J. H. *et al.* Dll1 marks early secretory progenitors in gut crypts that can revert to stem cells upon tissue damage. *Nat. Cell Biol.* (2012) doi:10.1038/ncb2581.Dll1.

12. Schonhoff, S. E., Giel-Moloney, M. & Leiter, A. B. Neurogenin 3-expressing progenitor cells in the gastrointestinal tract differentiate into both endocrine and non-endocrine cell types. *Dev. Biol.* (2004) doi:10.1016/j.ydbio.2004.03.013.

13. Gehart, H. & Clevers, H. Tales from the crypt: new insights into intestinal stem cells. *Nature Reviews Gastroenterology and Hepatology* (2019) doi:10.1038/s41575-018-0081-y.

14. Fre, S. *et al.* Notch signals control the fate of immature progenitor cells in the intestine.

Nature **435**, 964–968 (2005).

15. Yang, Q., Bermingham, N. A., Finegold, M. J. & Zoghbi, H. Y. Requirement of Math1 for secretory cell lineage commitment in the mouse intestine. *Science (80-.).* (2001) doi:10.1126/science.1065718.

16. Ritsma, L. *et al.* Intestinal crypt homeostasis revealed at single-stem-cell level by in vivo live imaging. *Nature* (2014) doi:10.1038/nature12972.

17. Takeda, N. *et al.* Interconversion between intestinal stem cell populations in distinct niches. *Science (80-.).* (2011) doi:10.1126/science.1213214.

18. Sangiorgi, E. & Capecchi, M. R. Bmi1 is expressed in vivo in intestinal stem cells. *Nat. Genet.* (2008) doi:10.1038/ng.165.

19. Montgomery, R. K. *et al.* Mouse telomerase reverse transcriptase (mTert) expression marks slowly cycling intestinal stem cells. *Proc. Natl. Acad. Sci. U. S. A.* (2011) doi:10.1073/pnas.1013004108.

20. Powell, A. E. *et al.* The pan-ErbB negative regulator lrig1 is an intestinal stem cell marker that functions as a tumor suppressor. *Cell* (2012) doi:10.1016/j.cell.2012.02.042.

21. Kozar, S. *et al.* Continuous clonal labeling reveals small numbers of functional stem cells in intestinal crypts and adenomas. *Cell Stem Cell* (2013) doi:10.1016/j.stem.2013.08.001.

22. Cortijo, C., Gouzi, M., Tissir, F. & Grapin-Botton, A. Planar Cell Polarity Controls Pancreatic Beta Cell Differentiation and Glucose Homeostasis. *Cell Rep.* (2012) doi:10.1016/j.celrep.2012.10.016.

23. Bader, E. *et al.* Identification of proliferative and mature beta-cells in the islets of Langerhans. *Nature* **535**, 430-+ (2016).

24. Roscioni, S. S., Migliorini, A., Gegg, M. & Lickert, H. Impact of islet architecture on β-cell heterogeneity, plasticity and function. *Nature Reviews Endocrinology* (2016) doi:10.1038/nrendo.2016.147.

25. Grumolato, L. *et al.* Canonical and noncanonical Wnts use a common mechanism to activate completely unrelated coreceptors. *Genes Dev.* (2010) doi:10.1101/gad.1957710.

26. Niehrs, C. The complex world of WNT receptor signalling. *Nature Reviews Molecular Cell Biology* (2012) doi:10.1038/nrm3470.

27. Gegg, M. *et al.* Flattop regulates basal body docking and positioning in mono- and multiciliated cells. *Elife* **3**, (2014).

28. Haber, A. L. *et al.* A single-cell survey of the small intestinal epithelium. *Nature* (2017) doi:10.1038/nature24489.

29. Muñoz, J. *et al.* The Lgr5 intestinal stem cell signature: Robust expression of proposed quiescent ' +4' cell markers. *EMBO J.* (2012) doi:10.1038/emboj.2012.166.

30. Lange, A. *et al.* FltpT2AiCre: A new knock-in mouse line for conditional gene targeting in distinct mono- and multiciliated tissues. *Differentiation* **83**, S105–S113 (2012).

31. Muzumdar, M. D., Tasic, B., Miyamichi, K., Li, N. & Luo, L. A global double-fluorescent cre reporter mouse. *Genesis* (2007) doi:10.1002/dvg.20335.

32. Burtscher, I., Barkey, W. & Lickert, H. Foxa2-venus fusion reporter mouse line allows live-cell analysis of endoderm-derived organ formation. *Genesis* (2013) doi:10.1002/dvg.22404.

33. Wolf, F. A. *et al.* PAGA: graph abstraction reconciles clustering with trajectory inference through a topology preserving map of single cells. *Genome Biol.* (2019) doi:10.1186/s13059-019-1663-x.

34. Kim, T. H. *et al.* Broadly permissive intestinal chromatin underlies lateral inhibition and cell plasticity. *Nature* (2014) doi:10.1038/nature12903.

35. Weinreb, C., Rodriguez-Fraticelli, A., Camargo, F. D. & Klein, A. M. Lineage tracing on transcriptional landscapes links state to fate during differentiation. *Science (80-.).* (2020) doi:10.1126/science.aaw3381.

36. Wagner, D. E. & Klein, A. M. Lineage tracing meets single-cell omics: opportunities and challenges. *Nature Reviews Genetics* (2020) doi:10.1038/s41576-020-0223-2.

37. Bastidas-Ponce, A. *et al.* Comprehensive single cell mRNA profiling reveals a detailed roadmap for pancreatic endocrinogenesis. *Dev.* (2019) doi:10.1242/dev.173849.

38. Curtin, J. A. *et al.* Mutation of Celsr1 disrupts planar polarity of inner ear hair cells and causes severe neural tube defects in the mouse. *Curr. Biol.* (2003) doi:10.1016/S0960-9822(03)00374-9.

Acknowledgements

We thank Kerstin Diemer, Jürgen Schultheiss, Ines Kunze, Anita Ludwig, and Anke Bettenbrock for excellent technical assistance, and Aurelia Raducanu and Pallavi Mahaddalkar for assistance with the FACS, and Henner Farin for teaching intestinal single cell culture. We are grateful to Jennifer Murdoch for providing *Celsr1*^{crsh} animals and Helena Edlund for providing the Ngn3 antibody. We thank Ralph Böttcher, Matthias Tschöp and Steve Woods for critical reading the manuscript.

This work was supported by an Emmy-Noether Fellowship and the European Union with the ERC starting grant Ciliary Disease [Project Number: 242807] and HumEn 7th Framework Programme FP7 Health -2013- Innovation 1 [Contract Number: 602889]. For financial support we would also like to thank the Helmholtz Society, Helmholtz Portfolio Theme 'Metabolic Dysfunction and Common Disease' (H.L. and J.B.), the Helmholtz Alliance 'Aging and Metabolic Programming, AMPro' (H.L., J.B.) and the Helmholtz Alliance ICEMED – Imaging and Curing Environmental Metabolic Diseases (H.L., J.B.). Further, this project was funded by ExNet-0041-Phase2-3 („SyNergy-HMGU")' through the Initiative and Network Fund of the Helmholtz Association (H.L., F.J.T.), by Helmholtz Association's Initiative and Networking Fund through Helmholtz AI [grant number: ZT-I-PF-5-01] (F.J.T.) and, the German Research Foundation and the German Center for Diabetes Research (DZD e.V.) (H.L.).

Authors Contributions A.B. designed experiments, performed experiments, analysed data and wrote the manuscript. M.B. analysed single-cell qRT-PCR and RNAseq data and helped writing the manuscript. S.T. analysed single-cell qRT-PCR data and helped writing the manuscript. M.S. analysed microarray data. A.A. performed western blot analysis of sorted cell populations. L.O. performed and analysed immunostainings. I.B. generated Ngn3-VF mouse line. S.S. analysed microarray data. M.I. and J.B. performed the microarrays and data analysis. C.Z. and W.E. contributed to single cell qRT-PCR experiment and discussions. A.C.S., F.M.V. and O.E. provided single-cell qRT-PCR resources and contributed to discussions. F.J.T. supervised M.B., S.T. and S.S. and analysed single-cell RNAseq and qRT-PCR data and helped writing the

manuscript. H.L. supported in study design, data analysis and writing and acquired financial support.

Competing interests

F.J.T. reports receiving consulting fees from Roche Diagnostics GmbH and Cellarity Inc., and ownership interest in Cellarity, Inc. and Dermagnostix. S.T. reports receiving consulting fees from Cellarity, Inc. All other authors declare no conflict of interest.

Methods

Animal studies. Animal experiments were carried out in compliance with the German Animal Protection Act and with the approved guidelines of the Society of Laboratory Animals (GV-SOLAS) and of the Federation of Laboratory Animal Science Associations (FELASA). This study was approved by the institutional Animal Welfare Officer and by the Government of Upper Bavaria, Germany. Mice were housed in groups of two to four animals and maintained at 23 ± 1 □C and 45-65 % humidity on a 12-hour dark/light cycle with ad libitum access to diet and water.

Mouse lines used:
Fltp^{ZV} (C57BL/6J)[27], *Fltp*^{T2AiCre} (mixed C57BL/6J, CD1 background)[30] crossed with *Gt(ROSA)26*^{mTmG} (mixed 129/SvJ, C57BL/6J background)[31], *Lgr5-EGFP-IRES-creERT2* (C57BL/6J)[1], Celsr1$^{Crsh/+}$ (mixed BALB/c, C57BL/6J background)[38], homozygous Ngn3-VF (mixed 129/SvJ, C57BL/6J background)[37], homozygous Foxa2$^{FVF/FVF}$ mice were generated as previously described and backcrossed to C57BL/6 background for at least 10 generations[32].
All experiments were performed using male and female 3-6-month-old mice.

Tissue preparation and immunohistochemistry
The intestine was isolated and flushed with ice-cold PBS, fixed with 4% paraformaldehyde (PFA) for 3h at 4°C and then placed for cryoprotection in a progressive sucrose gradient (7.5% sucrose for 1h, 15% sucrose for 1h, 30% sucrose overnight). Tissue was embedded in Optimum Cutting Temperature (Leica Biosystems, Germany, #14020108926) and sectioned at 14µm. Isolated intestinal crypts were fixed for whole-mount stainings with 4% PFA for 30min at room temperature (RT). After fixation crypts were washed three times with PBS. For immunofluorescence staining, sections or isolated crypts were permeabilized with 0.5 % Triton X-100 in PBS for 30 min at RT, blocked [(10% FCS, 0.1% BSA and 3% donkey serum in PBS/0.1 %Tween-20 (PBST)] for 1 h and incubated with primary antibodies overnight at 4 °C. Sections or crypts were washed in PBST, incubated with secondary antibodies in blocking solution for 1h at RT, followed by a DAPI (ROTH, 6335.1) staining to visualize the nuclei and mounted with the Elvanol antifade reagent.
For BrdU staining tissue was sectioned at 14µm and stained according to standard procedure followed by incubation in 3.3N HCl for 10min on ice, 50min at 37°C and incubation with borate buffer pH8.5 for 2x 15min at RT.

For stainings on single cells, cells were isolated by flow cytometry and cytospun on glass slides. Cells were dried and fixed with 4% PFA for 10min at RT, permeabilized with 0.25% Triton-X100 in PBS for 15min at RT and then blocked for 1h at RT followed by an overnight incubation with the primary antibody. Cells were washed in PBST, incubated with secondary antibodies in blocking solution for 1h at RT, followed by a DAPI (ROTH, 6335.1) staining to visualize the nuclei and mounted with the Elvanol antifade reagent. Sections, cells and crypts were visualized using a Leica SP5 confocal microscope.

The following primary antibodies were used for immunofluorescent stainings: chicken anti-GFP (1:600, Aves Labs, USA, GFP-1020); rat anti-BrdU (1:200, Abcam, ab6326); rat anti-RFP (1:500, Chromotek, ORD003515), goat anti-ChgA (1:200, Santa Cruz, sc-1488); rabbit anti-Lyz1 (1:1000, DAKO, A0099); rabbit anti-Muc2 (1:500, Santa Cruz, sc-7314); rabbit anti-Dclk1 (1:200, Abcam, ab37994); rat anti-BrdU (1:200, Abcam, ab6326); rabbit anti-Ki67 (1:200, Abcam, ab15580); rabbit anti-pJnk (1:100, NEB, #4668); rabbit anti-E-cadherin (extracellular domain) (1:1000, original source: Dietmar Vestweber). The following secondary antibodies were used: donkey anti-chicken Alexa Fluor 488 (1:800, Dianova, 703-225-155); donkey anti-mouse Cy5 (1:800, Dianova, 715-175-151); donkey anti-goat Alexa Fluor 555 (1:800, Invitrogen, A21432); donkey anti-rabbit Alexa Fluor 555 (1:800, Invitrogen, A31572); donkey anti-rabbit Alexa Fluor 649 (1:800, Dianova, 711-605-152); donkey anti-rat DyLight 549 (1:800, Dianova, #712-505-153).

pJnk fluorescence intensity analysis

Lgr5^{hi} and mTmG cells were isolated by flow cytometry and cytospun on glass slides. Cells were stained and imaged using a Leica SP5 Confocal microscope. Analysis was performed using the Leica LAS-AF (v2.6.0-7266) software. pJnk fluorescent intensity signal was determined from each cell and background signal was subtracted (secondary antibody only).

BrdU pulse-chase experiment

1mg/ml BrdU (Sigma, #B5002), in combination with 1% sucrose, was administered to mice via their drinking water for 14 days. BrdU-containing drinking water was exchanged every three days. Mice were sacrificed after 14 days of continuous BrdU labelling to assess the initial labelling efficiency and after a chase period of 10 and 21 days to assess label retention. Intestines were removed, flushed with ice-cold PBS, fixed with 4% PFA for 3h at 4°C, cryo-protected by a sucrose gradient and embedded in OCT. Cryosection imaging was performed using a Leica SP5 confocal microscope and cells were counted manually.

5-FU treatment

Intestinal injury was induced by injecting two intraperitoneal doses of 5-fluorouracil (5-FU, 100 mg/kg, Sigma) over a 48h period. Mice were sacrificed 48h or 26 days after the last 5-FU dose and intestinal tissue was analysed by immunohistochemistry and FACS. To assess the replication rate in the small intestine, 5-Ethynyl-2-deoxyuridine (EdU) (Thermo Fisher Scientific, A10044) was administered as an i.p. injection at 100 µg/g body weight from a 10 mg/ml stock in sterile PBS. Mice were sacrificed 4h post EdU administration. $Lgr5^{hi}$ and mTmG cells were isolated by flow cytometry and cytospun on glass slides. EdU staining was performed on cytopun cells using the Click-iT Staining Kit (Invitrogen, #C10340) according to the manufacturer's instructions.

Western blot analysis

For Western blot analysis, FVR^{+} and FVR^{-} cells were FAC-sorted and lysed in RIPA buffer (50mM Tris pH7.5, 150mM NaCl, 1mM EDTA, 1% Igepal, 0.1% SDS, 0.5% Sodium-deoxycholate) containing phosphatase inhibitor (Sigma-Aldrich, P5726, P0044) and proteinase inhibitor (Sigma-Aldrich, P8340). Cell lysates were resolved by SDS-PAGE, transferred to PVDF membrane (Biorad) and incubated with the following primary antibodies: rabbit anti-pJnk (1:1000, NEB, #4668); rabbit anti-Jnk (1:1000, NEB, #9258); mouse anti-Gapdh (1:5000, Merck Biosciences, CB1001); rabbit anti mTor (1:1000, Cell Signaling, #2972); rabbit anti-pmTor (Ser2448) (1:1000, Cell Signaling, #5536). Protein bands were visualized using horseradish peroxidase (HRP)-conjugated antibody, goat anti-mouse HRP (1:15000, Dianova, 115-036-062) or goat anti-rabbit HRP (1:15000, Dianova, 111-036-045) and chemiluminescence reagent (Millipore). The bands were quantified using ImageJ software v1.51.

Flow cytometry

For gene expression (microarray, single-cell RNAseq/qRT-PCR, qRT-PCR) analysis, Western Blot, and single-cell culture, crypt cells were sorted using the FACS-Aria III (FACSDiva software v6.1.3, BD Bioscience) and 100µm nozzle. For all experiments, single cells were gated according to their FSC-A (front scatter area) and SSC-A (side scatter area). Singlets were gated dependent on the FSC-W (front scatter width) and FSC-H (front scatter height) and dead cells were excluded using the 7-AAD staining solution (eBioscience, #00-6993-50).

Crypt isolation, crypt culture in matrigel, single-cell preparation for FACS, intestinal single-cell culture

Isolation and culture of small intestinal crypts and organoid culture was performed as previously described[39]. Briefly, intestines were harvested and washed with PBS. Villi were scraped away using coverslips. The remaining tissue was cut into 2cm pieces and incubated in 2mM EDTA/PBS for 35min at 4°C. Finally, crypts were collected by shaking. For Wnt-stimulation, isolated crypts were cultured in matrigel (BD Bioscience #356231) overlaid with medium containing 50ng/ml EGF (Life technologies PMG8043)/100ng/ml mNoggin (Peprotech, #250-38)/1µg/ml mR-spondin1 (R&D sytems, #2474-RS-050) (ENR) in the presence of 10µM Rock-inhibitor (Sigma, Y0503). Crypts were plated in 24-well plates at a density of 400 crypts/40µl matrigel. Two days after plating, the medium was changed for Wnt stimulation to ENR containing 400ng/ml Wnt ligand (Wnt5a, R&D systems #645-WN-010; Wnt11, R&D systems #6179-WN-010). After 2 days culture with Wnt ligands, crypts were intensively washed with ice-cold PBS and lysed in QIAzol (Qiagen, #79306) for RNA isolation (Qiagen, #79306) and cDNA synthesis (Invitrogen, SuperScript VILO cDNA synthesis kit, #11754).

For single-cell preparation, the crypt pellet was resuspended in 1-1,5ml TrypLE (Life technologies, #12605), incubated on ice for 5min, followed by 5min incubation at 37°C in a water bath. Then, 6ml of crypt complete medium containing 10% FCS and 10µg/ml DNase were added, and cells were incubated for 5min at 37°C in a water bath. The cells were gently resuspended by pipetting up and down 10 times, 10ml FACS buffer (2% FCS, 2mM EDTA in PBS) was added and the cells were centrifuged at 300xg, 5min, 4°C. Cells were washed twice with FACS buffer and finally the cell pellet was re-suspended in 1-2ml FACS buffer containing 10µM Rock-inhibitor (Sigma, Y0503), and cells were passed through the 40µm cell strainer caps of FACS tubes.

Single-cell culture to assess organoid formation efficiency, was performed as described previously[40]. 6,000 cells/25µl matrigel (BD Bioscience #356231) were seeded in a 24-well and overlaid with medium containing ENR, 10µM Rock-inhibitor (Sigma, Y0503), 1mM Valproic acid (Sigma, PHR1061) and 3µM CHIR99021 (Stemgent). Medium was changed every two days. VPA and CHIR99021 were added for the first 6 culture days. Bright-field images were acquired using a Zeiss microscope.

RNA isolation, qRT-PCR and microarray mRNA profiling

For gene profiling and qRT-PCR cells were directly sorted into Qiazol lysis reagent (Qiagen, #79306) and total RNA was extracted using the miRNeasy Micro kit (Qiagen, #217084)**,** RNA integrity was checked using Agilent 2100 Bioanalyzer (Agilent RNA 6000 Pico Kit) and cDNA was amplified with the Ovation PicoSL WTA System V2 in combination with the Encore Biotin Module (Nugen, USA). Amplified cDNA was hybridized on Affymetrix Mouse Gene 1.0 ST arrays (FVR) or Affymetrix Mouse Gene 2.0 ST arrays (Lgr5^{hi}/mTmG). Staining and scanning was performed according to the Affymetrix expression protocol, including minor modifications as suggested in the Encore Biotin protocol. For FVR data Expression Console (v.1.3.0.187, Affymetrix) was used for quality control and to obtain annotated normalized RMA gene-level data (standard settings including median polish and sketch-quantile normalisation). Lgr5^{hi}/mTmG data were RMA normalized using R/Bioconductor package oligo (version 1.38.0) and probesets were annotated using the R/Bioconductor package mogene20sttranscriptcluster.db (version 8.5.0). Differential expression analyses were performed with the R environment for statistical computing (R Development Core Team, http://www.R-project.org/) by using the limma package (version 3.30.7) and P-values were adjusted for multiple testing by Benjamini-Hochberg correction. A gene was considered as differentially expressed if the adjusted p-value (FDR) was below a threshold of 0.05 (for FVR) or <0.01 (for Lgr5^{hi}/mTmG; an additional filter for fold-change>2x was applied). Heatmaps were drawn using the pheatmap library for R. Expression is scaled row-wise and the colours range from dark blue (low expression) to orange (high expression). Functional enrichments were conducted using the GOstats package for R.

TaqMan qRT-PCR

TaqMan qRT–PCR was performed under standard conditions using ViiA7 (Applied Biosystems) and TaqMan Fast Advanced Master Mix (Applied Biosystems, #4444557) or TaqMan Universal Master Mix II (Applied Biosystems, #4440040) for amplified cDNA. Samples were normalized to housekeeping genes: 18S ribosomal RNA (*RN18S*) and glyceraldehyde 3-phosphate dehydrogenase (*Gapdh*).

Taqman probes (Applied Biosystems): *Lyz1*, Mm00657323_m1; *Chga*, Mm00514341_m1, *Gapdh*, Mm99999915_g1; *RN18S*, Mm03928990_g1; *Mki67*, Mm01278617_m1; *Cdkn1a* (p21), Mm04205640_g1; *Muc2*, Mm01276696_m1; *Ccnd1*, Mm00432359_m1; *Ror2*, Mm01341765_m1/ Mm00443470_m1; *Fltp*, Mm01290543_g1; *Fltp*, Mm01290541_m1

Prickle1, Mm01297035_m1; *Dvl2*, Mm00432899_m1; *Celsr1*, Mm00464808_m1; *Fzd6*, Mm00433387_m1; *Jun*, Mm00495062_s1.

Single-cell gene expression analysis by microfluidic qRT-PCR

Small intestinal crypt cells were kept cold and sorted using FACS-Aria III (BD Bioscience). Doublets were excluded and dead cells were excluded using 7-AAD (eBioscience, #00-6993-50). The pre-amplification solution in 96-wells included 5µl of a master mix containing 1.2µl 5x VILO reaction mix (Invitrogen, #11754-050), 0.3µl 20U/µl SUPERase-In (Ambion, #AM2694), 0.25µl 10% NP40 (Thermo Scientific, #28324), 0.25µl RNA spikes mix (Fluidigm, #100-5582) and 3 µl nuclease-free water (Promega, #P119C). Cells were lysed by incubation at 65°C for 90s and RNA was transcribed into cDNA by adding 1µl of RT mix solution containing 0.15µl 10x SuperScript enzyme mix (Invitrogen, #11754-050), 0.12µl T4 Gene 32 Protein (New England BioLabs, #M0300S) and 0.73 µl nuclease-free water and RT cycling (25°C for 5min, 50°C for 30min, 55°C for 25min, 60°C for 5min and 70°C for 10min). Target specific cDNA amplification was performed by adding 9µl reaction mix containing 7.5µl TaqMan PreAmp Master Mix (Applied Biosystems, #4391128), 0.075µl 0.5M EDTA, pH 8.0 (Invitrogen, #Am9260G), 1.5µl 10x outer primer mix (500nM) (see Supplementary Table 4) and 20 cycles of denaturation for 5s at 96°C and 4 min annealing/extension at 60°C following an enzyme activation step at 95°C for 10min. Exonuclease I treatment was performed to clean up the reaction by adding a 6µl reaction mix containing 0.6µl reaction buffer, 1.2µl Exonuclease I (New England BioLabs, #M0293S) and 4.2µl nuclease-free water.

Amplified single-cell cDNAs were analysed with gene specific inner primer pairs (Supplementary Table 4) and SsoFast EvaGreen Supermix with Low ROX (Bio-Rad Laboratories, #172-5210) using the 96 × 96 Dynamic Array on the BioMark System (Fluidigm). Ct values for each gene in each cell was calculated using BioMark Real-Time PCR Analysis software v3 (Fluidigm) (Supplementary Table 5).

Computational analyses of single-cell qRT-PCR data

We manually removed 8 cells due to technical problems (pipetting error) during experimental processing. Samples were then corrected for deviating sample dilution of PCR runs. We followed the normalization procedure as suggested in[41]. Briefly, we subtracted Ct values from the assumed limit of detection of the BioMark (LOD=30). As quality control measure and reference we used the expression values of the three most robustly expressed housekeeping

genes *Rn18S*, *ActB* and *Hsp90*. We excluded all cells that did not express all three housekeepers as well as cells for which the mean of the three housekeepers was ±3 s.d. from the mean of all cells. ΔCt values were then normalized on a cell-wise basis to the mean expression of the three housekeeping genes. The minimum of the normalized data - 2 was then assigned as a ΔCt value where a gene was not detected (failed qPCR runs). 595 of 672 sorted cells were retained for further analysis. *Foxa1*, *Foxa2*, *GFP* did not amplify correctly in one run so these genes have been excluded from the analysis as were all housekeeping genes (*Rn18S*, *ActB*, *Hsp90*, *Uba52*, *Gapdh*, *Rpl37*). We quantified three synthetic RNAs of different concentrations to explore its use as a reference. The signals of the RNA spikes were too strong and not quantifiable in all experimental runs and were therefore removed before further analyses. *Fltp* was detected in the negative control of Neurog3 cells and therefore had to be excluded from multivariate analyses. For the other cell types *Fltp* measurements were correct. In total, we used ΔCt values of 80 genes. All further analysis of single-cell qPCR data was performed using Scanpy (v.1.0.4) and Python 3.5 and 3.6, respectively. The single-cell neighborhood graph was computed on the 15 first principal components with a local neighborhood size of 5 (pp.pca and pp.neighbors) and UMAP was run for visualization (tl.umap). Louvain-based clustering at a resolution of 0.8 was used for subtype identification which were annotated based on the expression of known marker genes (pp.louvain). Genes characteristic for each subtype were identified using a wilcoxon-ranksum test (tl.rank_gene_groups). Top 5 ranked genes were considered for plotting. For the reconstruction of lineage relationships and differentiation trajectories we used PAGA (tl.paga) and diffusion pseudotime (dpt, tl.dpt). We first applied PAGA to find the branching into the EEC and Paneth cell lineage. For each lineage (branch in PAGA) we then arranged cells by their pseudotemporal order inferred from dpt (pl.paga_path). The root is represented by a cell in the ISC population, defined as $Lgr5^+$ cells expressing the stem cell markers (*Lgr5*, *Olfm4*, *Ascl2*, *Axin2* and *Prom1*) but without specific lineage markers (*Lyz1*, *Mmp7*, *Atoh1*, *Dll4*, *Dll1* or *Sis*). Random variation of the root within the stem cell population did not substantially change dpt. Expression values along a trajectory are plotted as the smoothed average over n cells using a sliding window with Gaussian noise as implemented in pl.paga_path (n as indicated in figure legend).

Single-cell RNA sequencing: RNA preparation, library generation and sequencing.

Samples from SI crypts were prepared as described above under section crypt isolation and flow cytometry. For rare lineage enrichment live crypt cells were mixed with reporter positive cells at different ratios. Number of dead cells was estimated by trypan blue staining and sorted cells were counted. Single-cell libraries were generated using the Chromium™ Single cell 3' library and gel bead kit v2 (10X Genomics, #120237) according to the manufacturer's instructions. Libraries were sequenced on the HiSeq4000 (Illumina) with 150 bp paired-end sequencing of read 2.

Computational analysis

Pre-processing of droplet-based scRNAseq data

De-multiplexing and alignment to mm10 mouse genome, identification of unique molecular identifiers (UMI) and barcode filtering was performed using the 'CellRanger' toolkit (version 2.0.0) provided by 10X Genomics. We performed a further barcode (=cell) selection step and additionally included cells with more than 1000 expressed genes, where a gene is counted as expressed if we found at least one UMI mapped to it. We further filtered cells with a fraction of counts from mitochondrial genes > 10% indicative for stressed or dying cells.

We removed doublets by computing the doublet score from *scrublet*[42] on the UMI count matrix separately for every sample. Using a threshold of 0.4, we removed 1651 cells from the analysis.

Cells from all samples were log-normalised and batch corrected using ComBat as Python implementation. Please note that we observed an overrepresentation of Paneth cells in the FVR-enriched samples (with 50% and 90% enrichment, resp.), where we subsampled the Paneth cell populations to 15% to fit the cell-type distribution of all other samples before we corrected with ComBat. Then, we used the pre-computed regression coefficients to correct for batch effects in the filtered cells and merged them with the full data set. Further, we fixed all zero values to remain zero in order to preserve the support of the count data. We computed the top 2000 highly variable genes based on mean and dispersion (pp.filter_genes_dispersion in SCANPY v. 1.3.1 in Python 3.6 with the flavor 'cell_ranger' to compute normalised dispersions[43]).

Further, we corrected for the library size by scaling the reads per cell to the factor 100,000 (pp.normalize_per_cell in SCANPY v. 1.3.1 in Python 3.6).

Dimension reduction

We performed our analyses with SCANPY[44] v. 1.3.1 in Python 3.6. We used a UMAP[45] to represent the data in the two-dimensional embedding and data visualisation (tl.umap). This was created based on a PCA-space with n=50 components, and the k-nearest neighbour graph on the PCA-space with k=30 (tl.pca and pp.neighbors). PCA etc. was computed on the scaled and normalised data with 2,000 highly variable genes.

Clustering and cell type annotation

We determined the clustering and cell type annotation for the control samples as follows. We inspected first marker gene expression for respective major cell types and computed gene scores using known marker genes (tl.score_genes, based on ref.[46]). Analogously, we computed a cell cycle score to determine the respective cell-cycle phase state of the cells (tl.score_genes_cell_cycle, based on ref.[46]). Then, we performed clustering using the louvain algorithm[47] (tl.louvain with default resolution parameter 1.0) and found 18 clusters. Here, we annotated and merged clusters again according to the gene scores and marker gene expression. Here, we also identified 1589 immune cells, which were distinct from the remaining cells.

Subsequently, we inspected all main clusters for substructure and resolved it further based on marker gene expression. Here, we used louvain clustering with resolution parameters ~1-2 and merged the subclusters again according to marker gene expression (hierarchical 'split-and-merge' approach). Finally, we annotated 7 major cell types (ISC, Enterocytes, Goblet cells, Paneth cells, Enteroendocrine cells and Tuft cells), subdivided them into progenitor and mature cells. In the ISC population, we identified a PC-primed ISC population that was more similar to the Paneth progenitor population.

For the mutant samples, we employed a k-nearest neighbour approach to match every cell to the corresponding cluster (k=30), i.e. we derived the cell identity of the mutants from the cell identity of neighbouring cells of the control samples, which we annotated beforehand. Again, we identified 2289 immune cells, which we removed from analysis.

Differential expression analysis

We used the limma package[48] (version 3.34.9 in R 3.4.3) to study differential expression. First, we excluded the FVF enriched samples and mutant samples. In order to determine differentially expressed genes between ISCs and progenitor populations, we tested pairwise progenitor populations vs ISC (without Paneth primed ISCs) and Paneth progenitors vs Goblet progenitors. Please note that differential expression was performed on the log-

normalised (not batch-corrected) data, where we included the sample information (i.e. batch) as covariate. In addition, we excluded all genes with mean expression < 0.05. We considered only significant genes (FDR<0.05) with logFC>0.05. For the analysis of transcription factors, we filtered differentially expressed transcription factors (gene ontology ID GO:0003700 (transcription factor activity)) with the biomartr package[49] (version 0.7.0 in R 3.4.3) with a p-value threshold $p_{adj}<10^{-5}$.

Analogously, in order to determine differentially expressed genes between mutants and control samples (without FVF enriched samples), we tested every cluster separately with limma. Please note that differential expression was performed on the log-normalised (not batch-corrected) data, where we included the number of expressed genes as covariate, but not the sample information (i.e. batch) due to confounding of genetic condition and sample covariates. In addition, we excluded all genes with mean expression < 0.05. We considered only significant genes (FDR<0.05) with logFC>0.05. For the analysis of transcription factors, we filtered differentially expressed transcription factors (gene ontology ID GO:0003700 (transcription factor activity)) with the biomartr package (version 0.7.0 in R 3.4.3) and with an adjusted p-value threshold $p_{adj}<10^{-5}$ (Benjamini-Hochberg correction).

Identifying cell differentiation trajectories via graph abstraction

To derive cell trajectories, we computed a pseudotemporal ordering using diffusion pseudotime (DPT, tl.dpt in SCANPY)[50]. As the topology of the data is complex, we used partition-based graph abstraction (PAGA)[33] to quantify the connections between the clusters (*i.e.* connections of ISCs to respective progenitors and mature cell types, tl.paga in SCANPY). We display all connections with a scaled connectivity of at least 0.05 ('threshold' parameter in pl.paga in SCANPY).

Gene Set Enrichment Analysis

We performed a gene set enrichment analysis based on both GO[51,52] terms and KEGG[53] terms using g:profiler[54]. In particular, we adapted the Python wrapper from V. Svensson (https://github.com/vals/python-gprofiler). We set the background to all expressed genes and removed all resulting gene sets with significance level p>=0.05. Further, we split the input data set by the sign of the log-fold change, such that we considered up-regulated and down-regulated gene sets separately in each set of differentially expressed genes. For visualisation of gene set significance, we abridged p-values at 10^{-10}.

Code availability

Custom R scripts of the single-cell qRT-PCR bioinformatics analysis are available in a jupyter notebook upon request.

Single-cell RNAseq analysis is available under https://github.com/theislab/gut_lineage/.

Data availability

Microarray data have been deposited in NCBI/GEO under accession code GSE94092.

scRNAseq data have been deposited in NCBI/GEO under accession code GSE152325.

Otherwise, all data generated or analysed during this study are included in this manuscript (and its supplementary information files).

Statistical analysis and reproducibility

No statistical methods were used to predetermine sample size. The experiments were not randomized and the investigators were not blinded to allocation during experiments and outcome assessment.

Data collection was performed using Microsoft office excel 2016-2018 and statistical analysis was performed using GraphPad Prism 6 Software (GraphPad Software, USA). Data are expressed as mean values with error bars (s.d. or s.e.m., as indicated in the figure legends) and were compared using unpaired t-tests unless indicated otherwise. The number of times an experiment was repeated is indicated in the figure legends.

References

39. Andersson-Rolf, A., Fink, J., Mustata, R. C. & Koo, B. K. A video protocol of retroviral infection in primary intestinal Organoid culture. *J. Vis. Exp.* (2014) doi:10.3791/51765.

40. Yin, X. *et al.* Niche-independent high-purity cultures of Lgr5 + intestinal stem cells and their progeny. *Nat. Methods* (2014) doi:10.1038/nmeth.2737.

41. Moignard, V. *et al.* Decoding the regulatory network of early blood development from single-cell gene expression measurements. *Nat. Biotechnol.* (2015) doi:10.1038/nbt.3154.

42. Wolock, S. L., Lopez, R. & Klein, A. M. Scrublet: Computational Identification of Cell Doublets in Single-Cell Transcriptomic Data. *Cell Syst.* (2019) doi:10.1016/j.cels.2018.11.005.

43. Zheng, G. X. Y. *et al.* Massively parallel digital transcriptional profiling of single cells. *Nat. Commun.* (2017) doi:10.1038/ncomms14049.

44. Wolf, F. A., Angerer, P. & Theis, F. J. SCANPY: Large-scale single-cell gene expression data analysis. *Genome Biol.* (2018) doi:10.1186/s13059-017-1382-0.

45. McInnes, L., Healy, J., Saul, N. & Großberger, L. UMAP: Uniform Manifold Approximation and Projection. *J. Open Source Softw.* (2018) doi:10.21105/joss.00861.

46. Satija, R., Farrell, J. A., Gennert, D., Schier, A. F. & Regev, A. Spatial reconstruction of single-cell gene expression data. *Nat. Biotechnol.* (2015) doi:10.1038/nbt.3192.

47. Blondel, V. D., Guillaume, J. L., Lambiotte, R. & Lefebvre, E. Fast unfolding of communities in large networks. *J. Stat. Mech. Theory Exp.* (2008) doi:10.1088/1742-5468/2008/10/P10008.

48. Ritchie, M. E. *et al.* Limma powers differential expression analyses for RNA-sequencing and microarray studies. *Nucleic Acids Res.* (2015) doi:10.1093/nar/gkv007.

49. Drost, H. G. & Paszkowski, J. Biomartr: Genomic data retrieval with R. *Bioinformatics* (2017) doi:10.1093/bioinformatics/btw821.

50. Haghverdi, L., Buttner, M., Wolf, F. A., Buettner, F. & Theis, F. J. Diffusion pseudotime robustly reconstructs lineage branching. *Nat. Methods* **13**, 845-+ (2016).

51. Ashburner, M. *et al.* Gene ontology: Tool for the unification of biology. *Nature Genetics* (2000) doi:10.1038/75556.

52. Carbon, S. *et al.* Expansion of the gene ontology knowledgebase and resources: The gene ontology consortium. *Nucleic Acids Res.* (2017) doi:10.1093/nar/gkw1108.

53. Kanehisa, M., Sato, Y., Kawashima, M., Furumichi, M. & Tanabe, M. KEGG as a reference resource for gene and protein annotation. *Nucleic Acids Res.* (2016) doi:10.1093/nar/gkv1070.

54. Reimand, J. *et al.* g:Profiler-a web server for functional interpretation of gene lists (2016 update). *Nucleic Acids Res.* (2016) doi:10.1093/nar/gkw199.

Böttcher et al. Figure 1

FVR labels the secretory enteroendocrine and Paneth cell lineages.

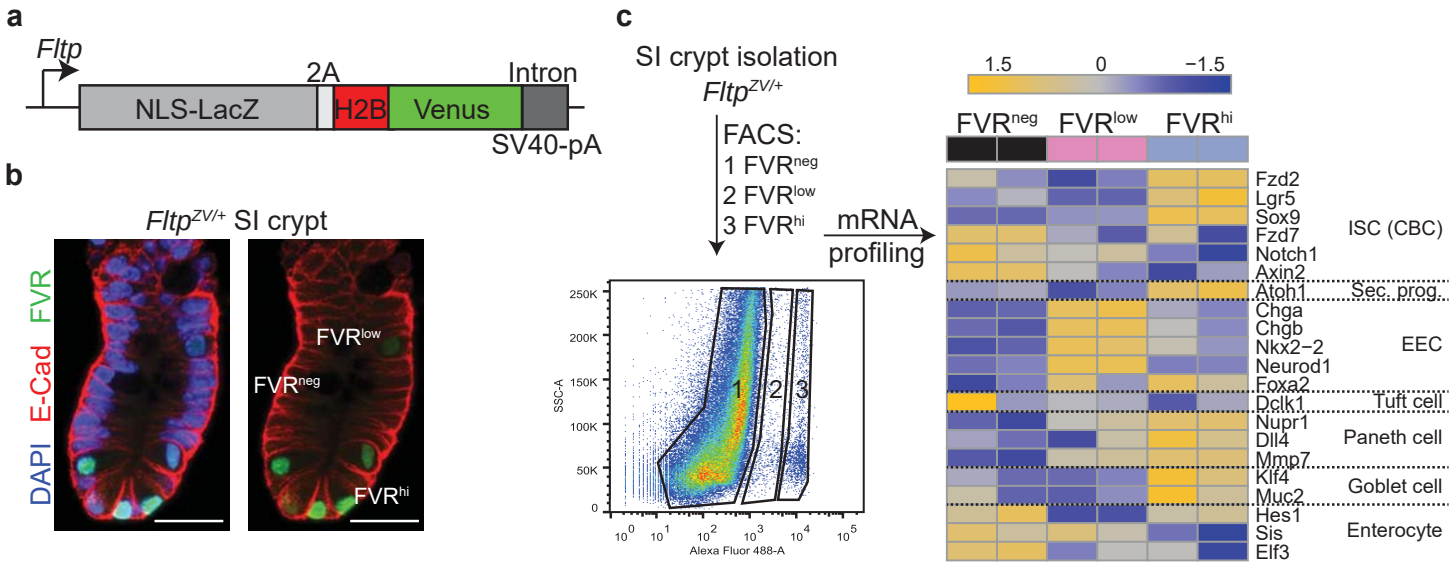

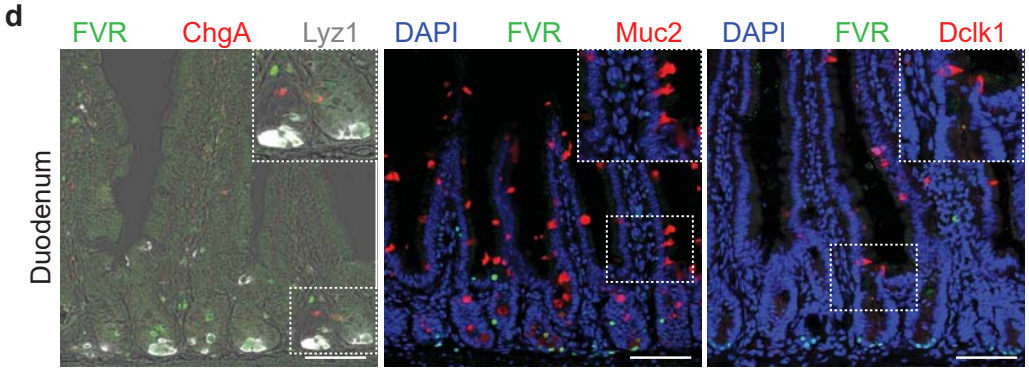

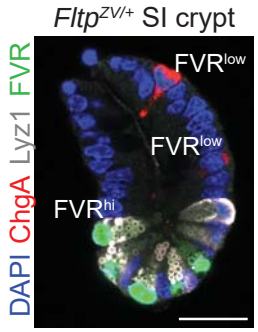

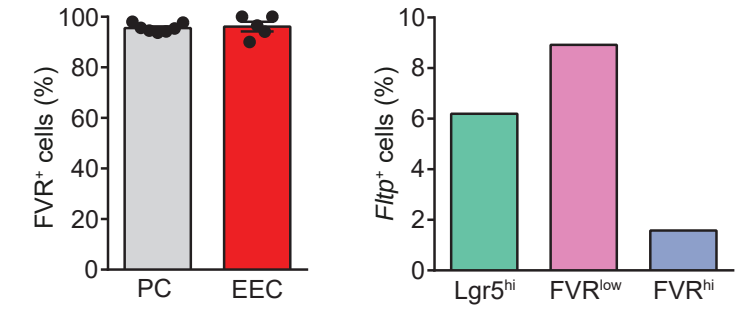

Böttcher et al. Figure 2

Wnt/β-catenin and Wnt/PCP activated Lgr5⁺ ISCs are indistinguishable at the transcriptional level.

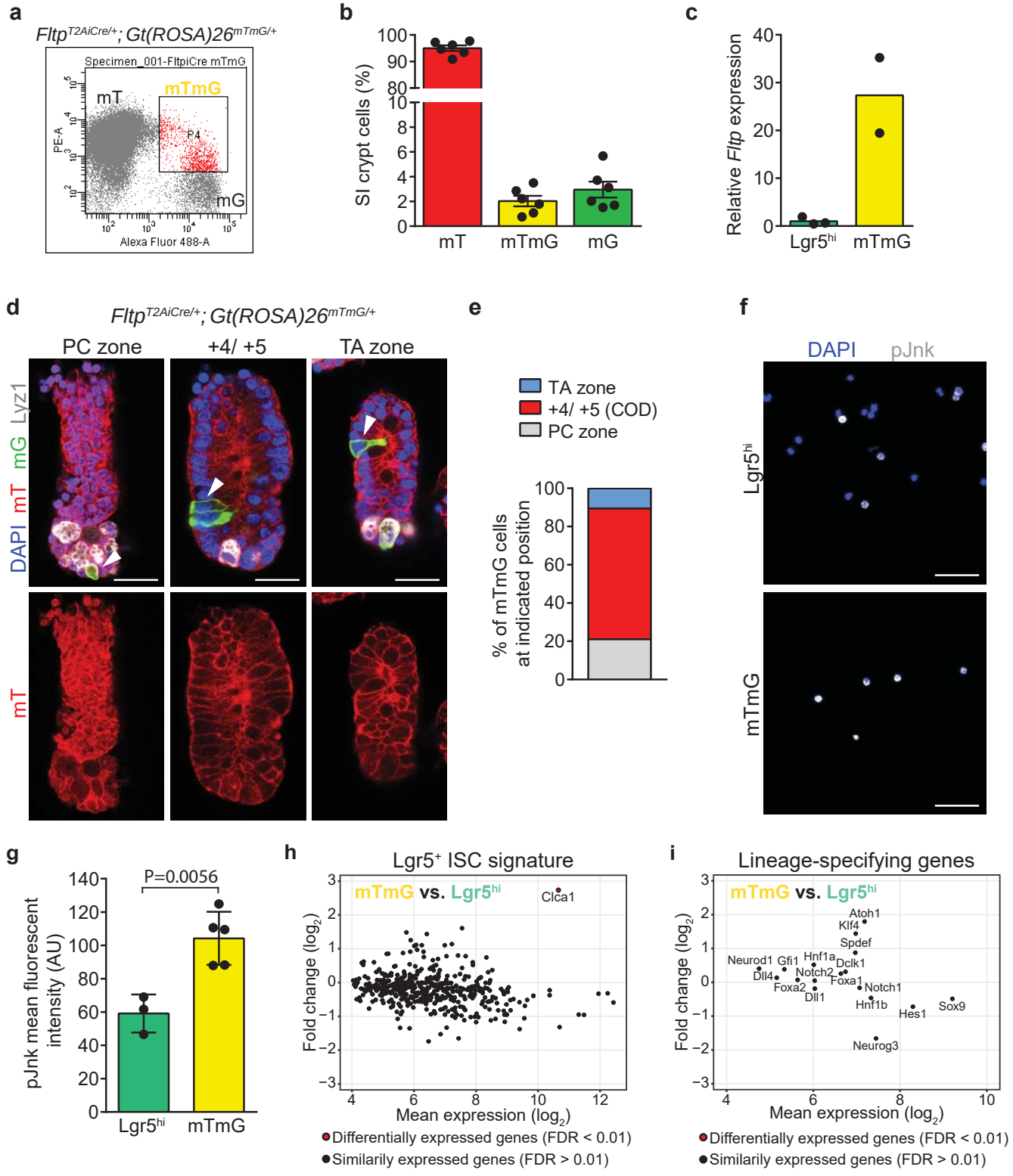

Böttcher et al. Figure 3

Subtype enrichment of crypt cells reveals distinct progenitor states for all intestinal lineages.

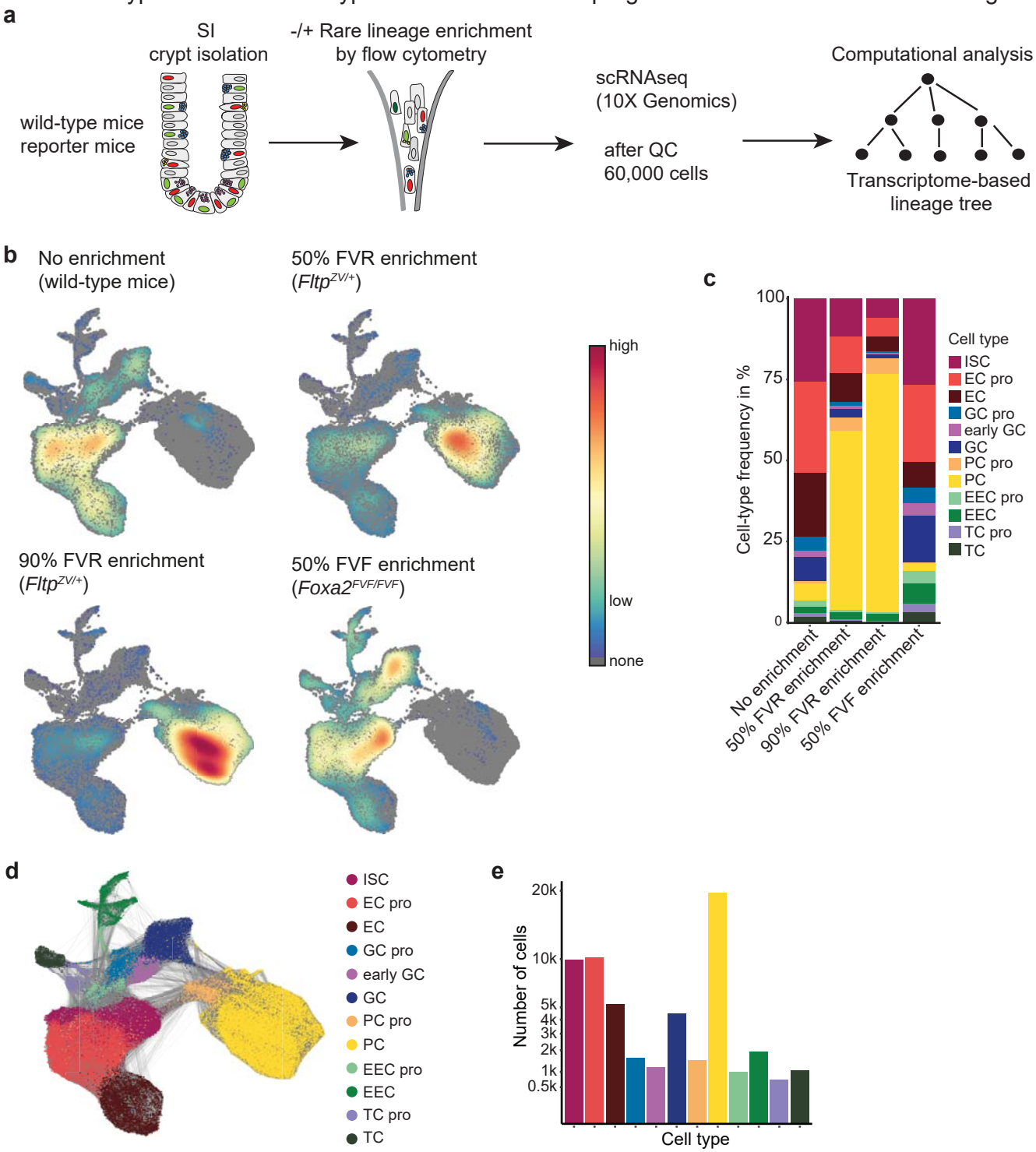

Böttcher et al. Figure 4

Temporal-resolved lineage labelling and pseudotemporal ordering of intestinal crypt cells shows that EECs and PCs directly allocate from ISCs via unipotent transition states.

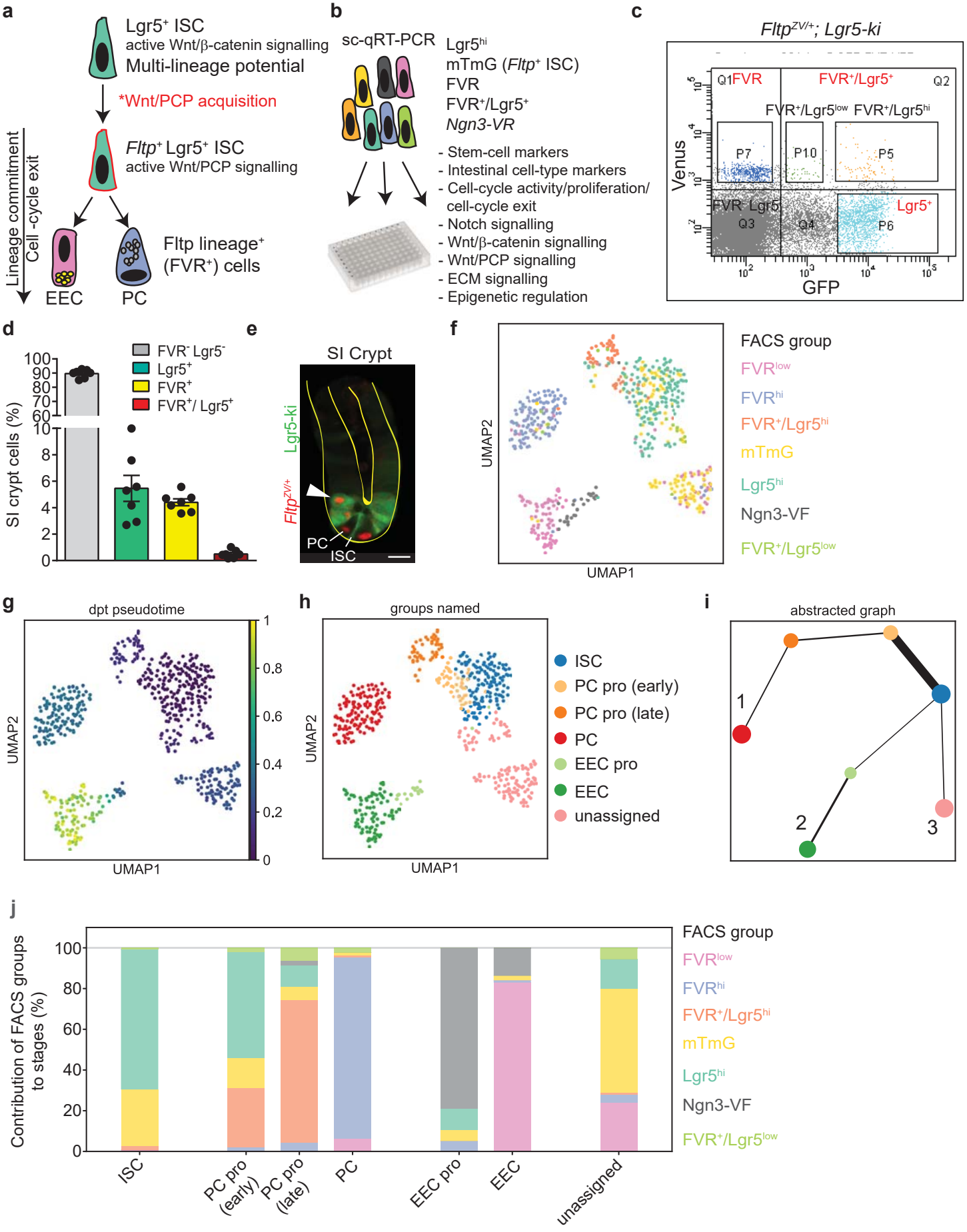

Böttcher et al. Figure 5

FVR marks Lgr5+ label-retaining cells that give rise to Paneth cells.

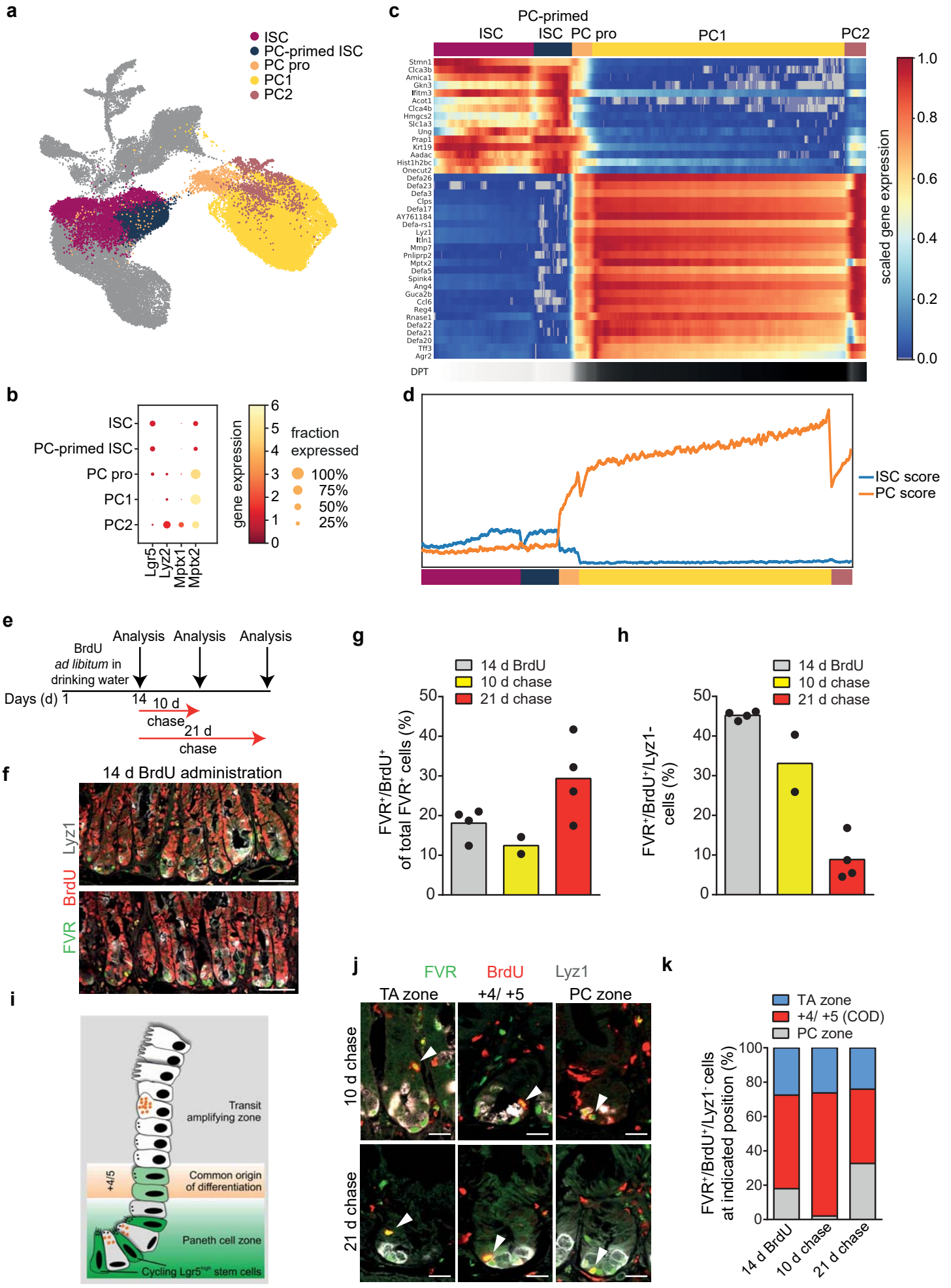

Böttcher et al. Extended Data Figure 1

FVR labels all Paneth and enteroendocrine subtypes.

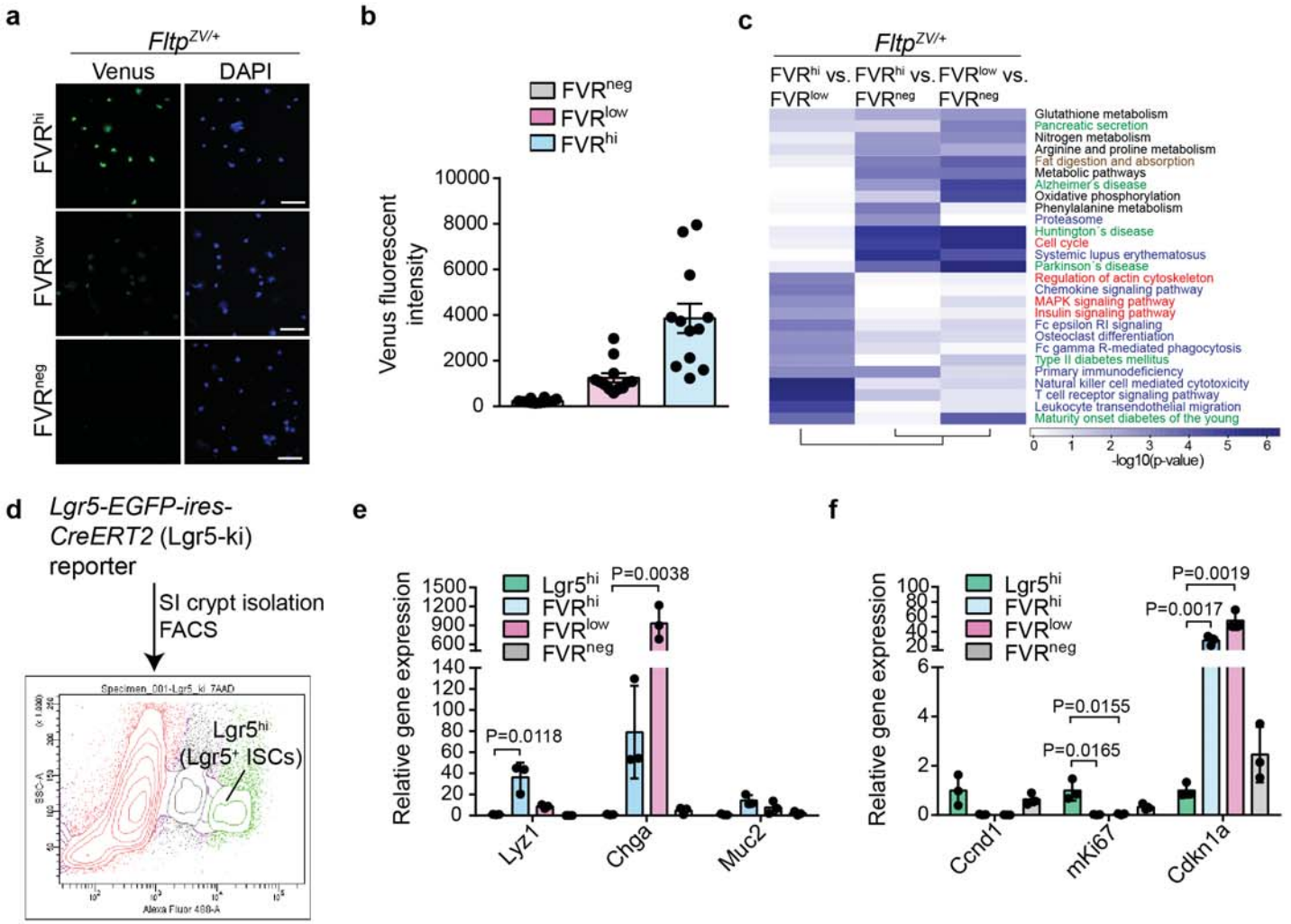

Böttcher et al. Extended Data Figure 1

FVR labels all Paneth and enteroendocrine subtypes.

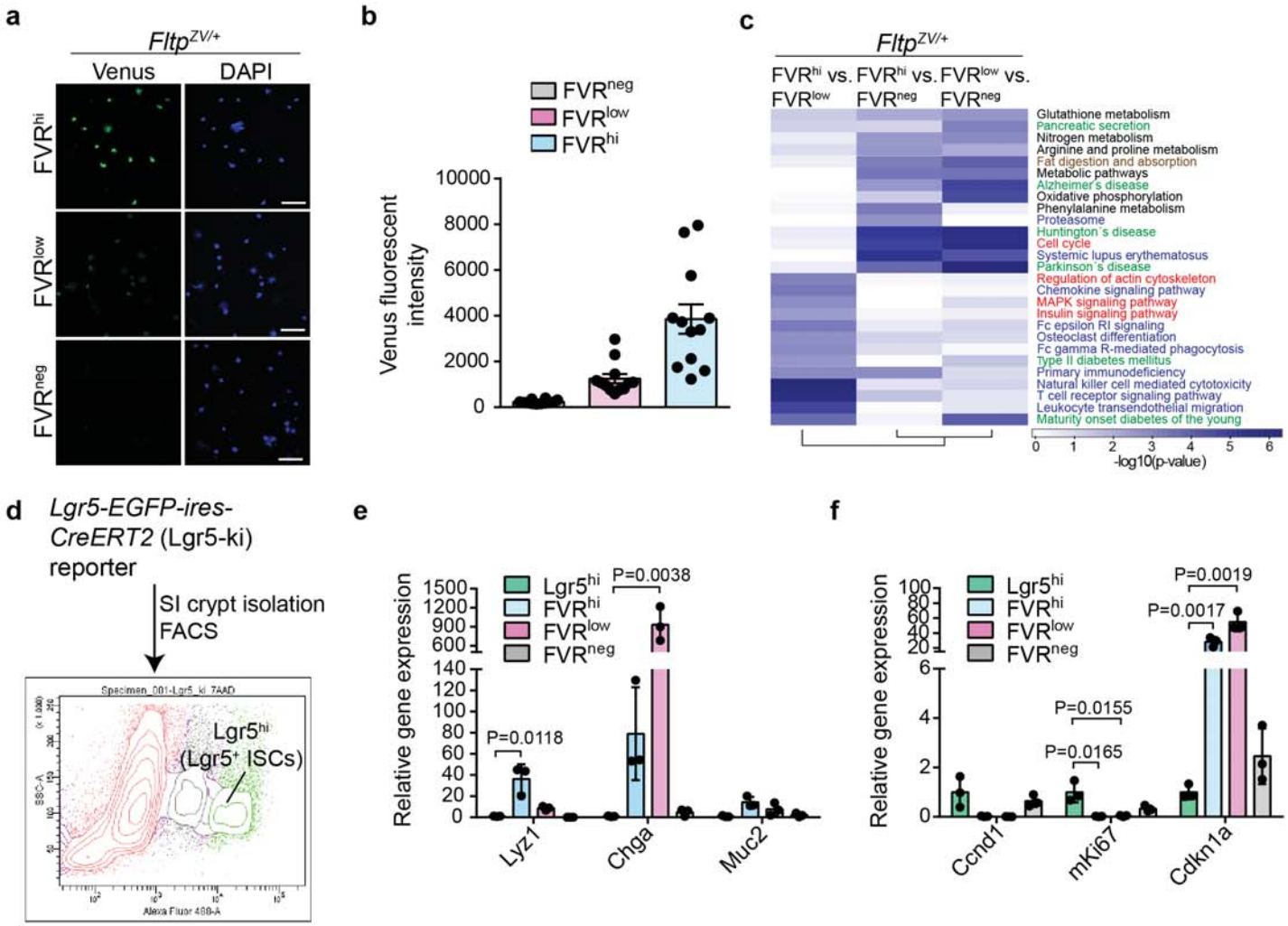

Böttcher et al. Extended Data Figure 2

Fltp⁺ cells possess limited organoid forming capacity *in vitro*.

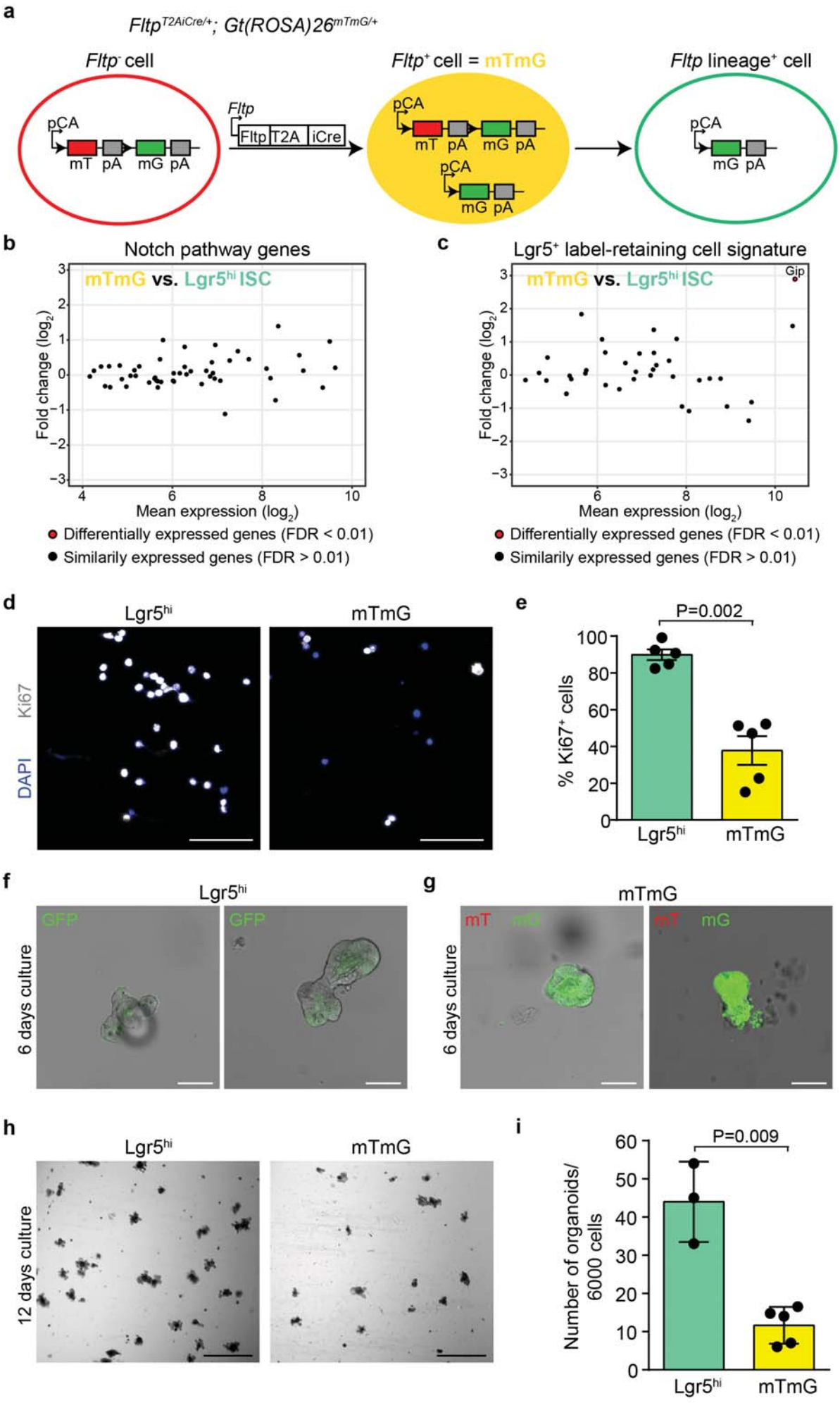

Böttcher et al. Extended Data Figure 3

Fltp⁺ cells possess limited multi-lineage potential *in vivo*, are resistant to chemical injury but do not contribute to regeneration after intestinal injury.

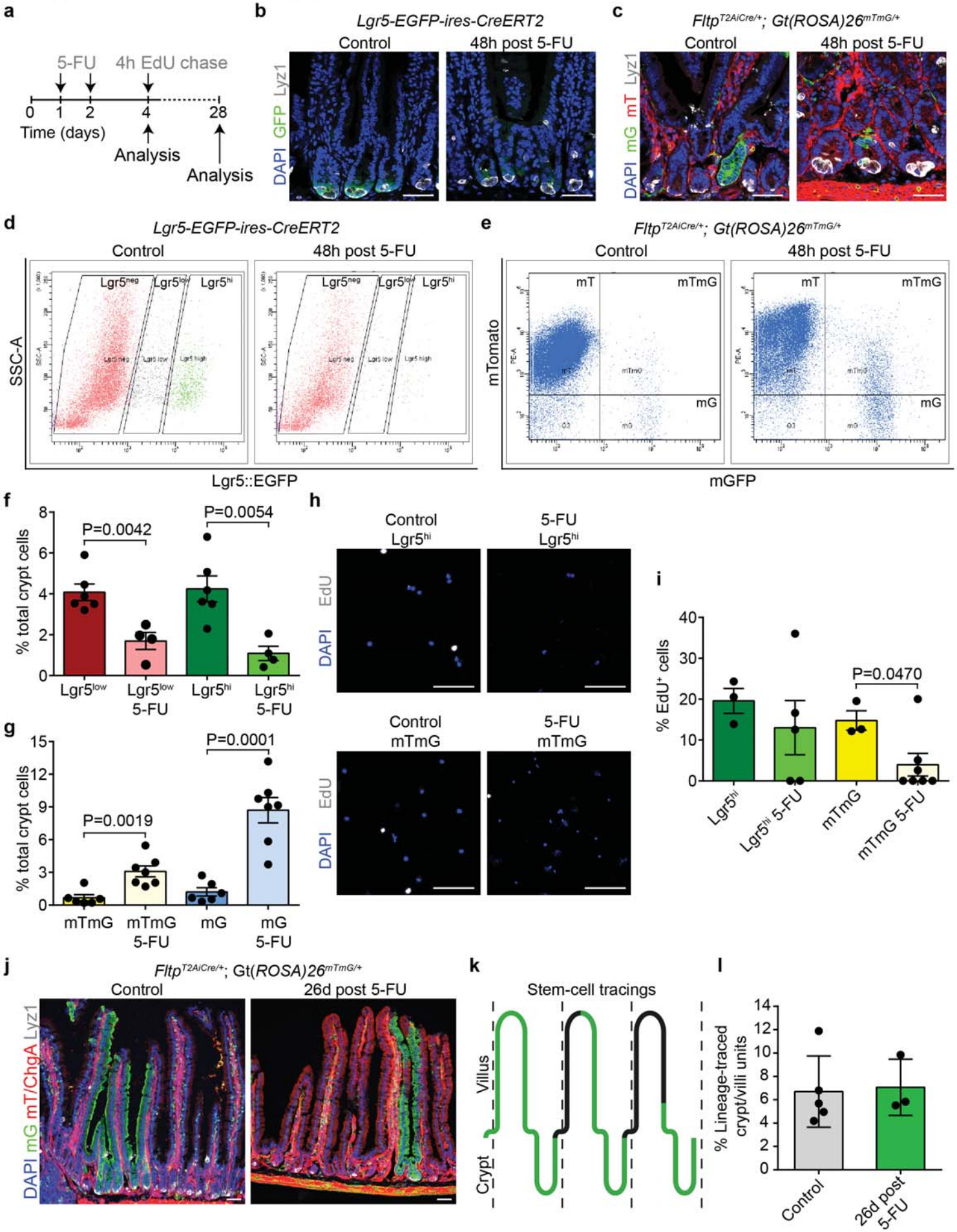

Böttcher et al. Extended Data Figure 4

Identification of progenitors for each intestinal lineage by scRNAseq.

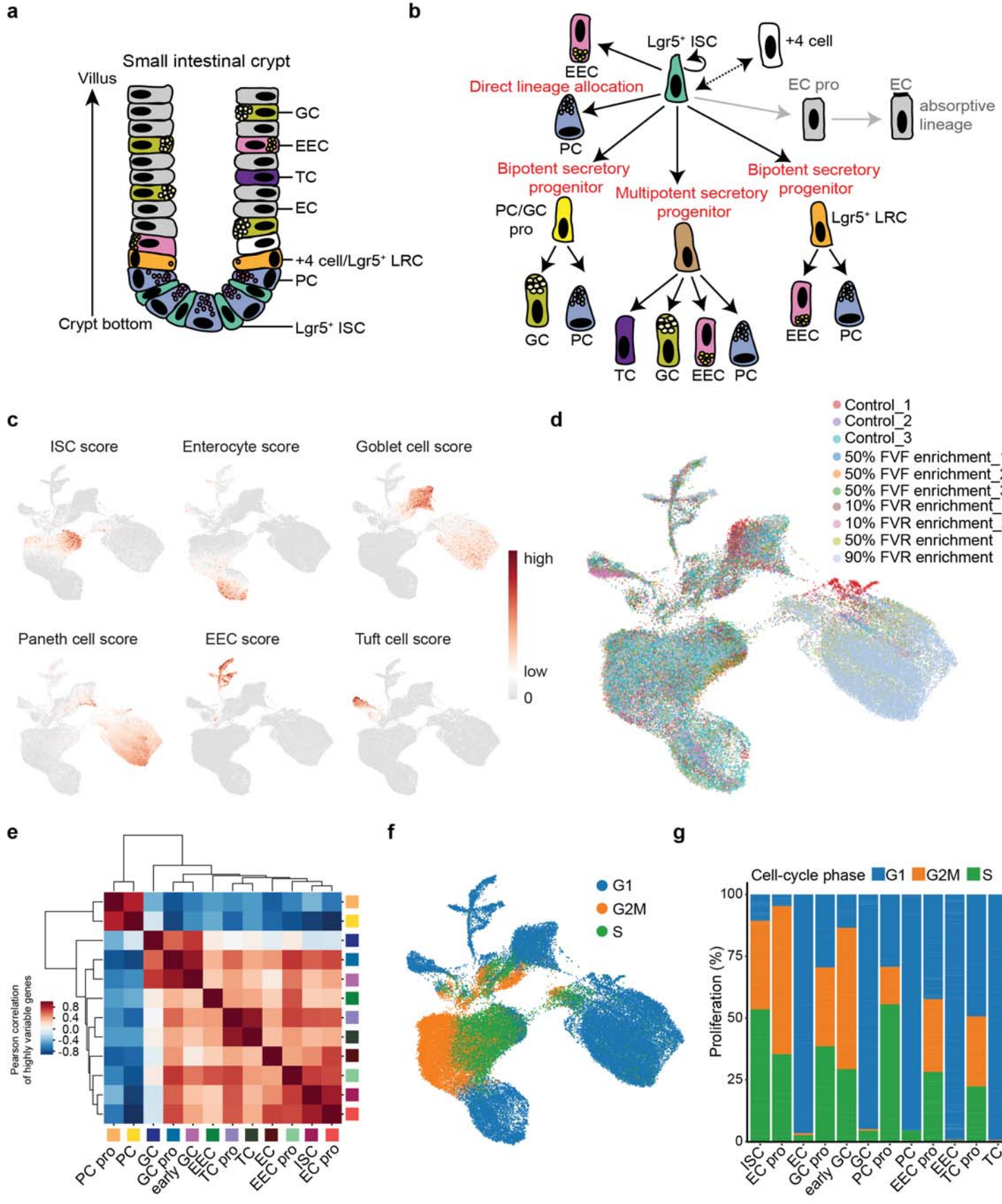

Böttcher et al. Extended Data Figure 5

Intestinal progenitors are characterized by distinct gene expression patterns.

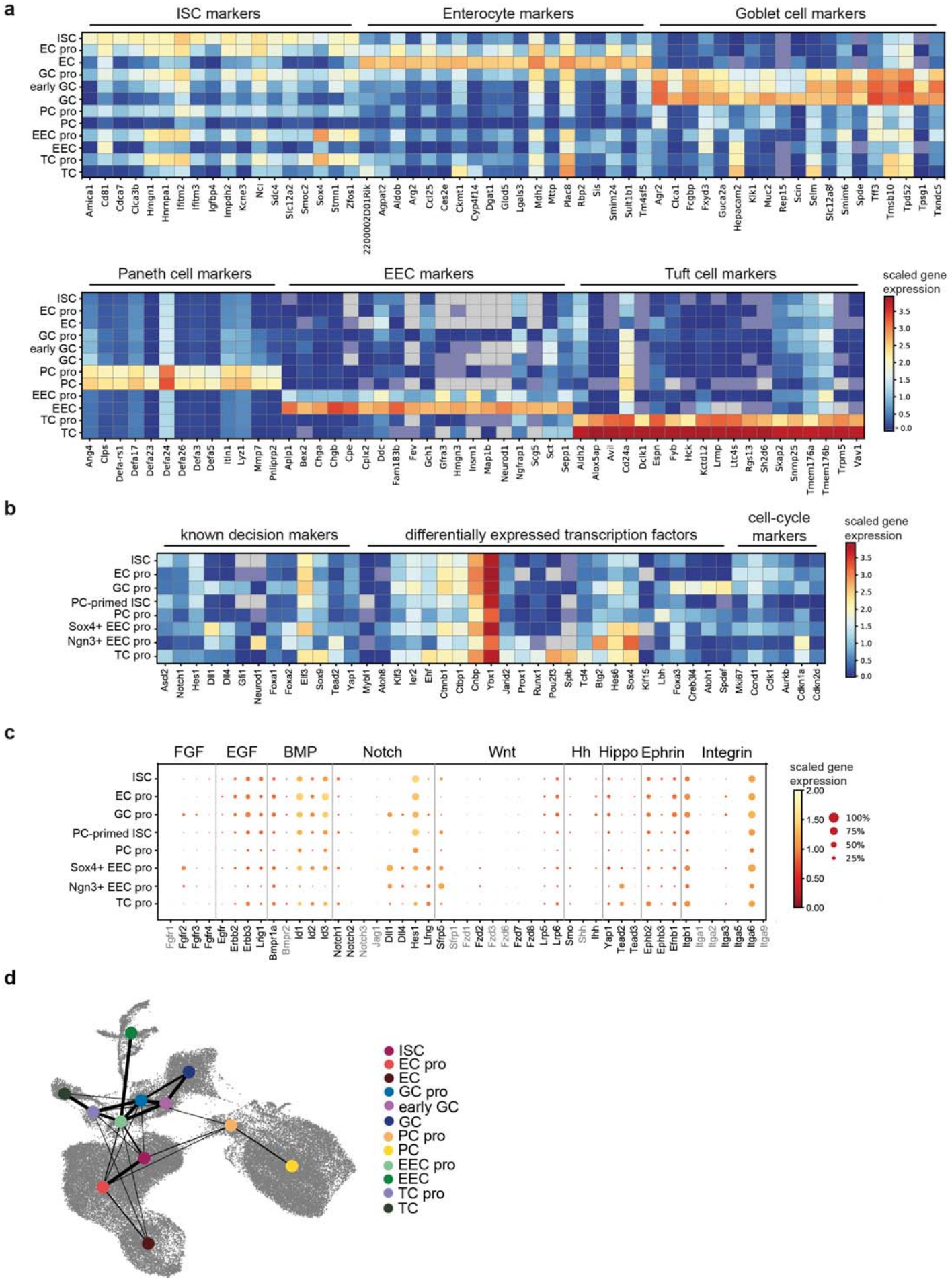

Böttcher et al. Extended Data Figure 6

Pseudotemporal ordering of cells identifies unipotent transition states for EEC and PC lineage formation characterized by downregulation of stem-cell and co-expression of stem-cell and secretory lineage genes, respectively.

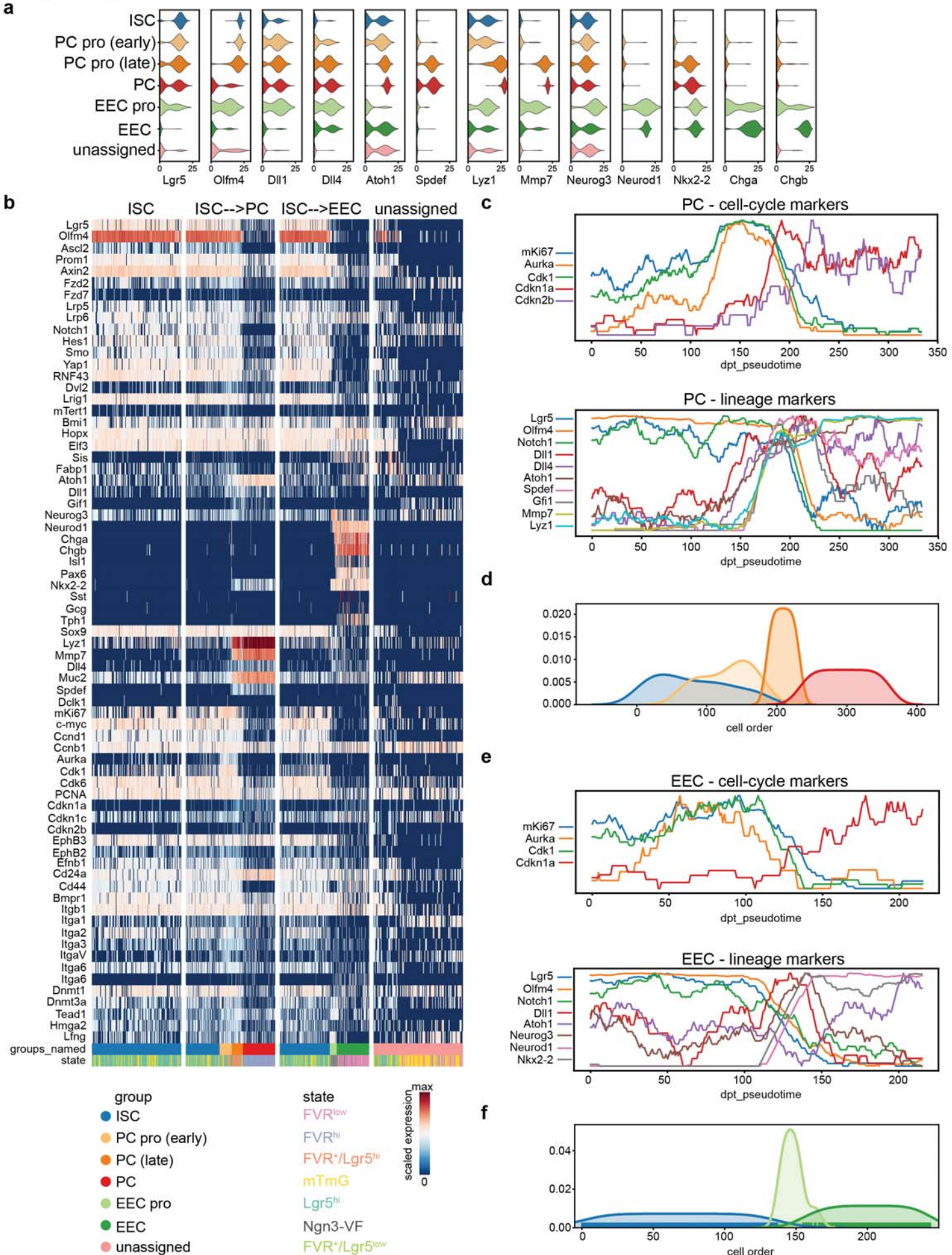

Böttcher et al. Extended Data Figure 7

Non-canonical Wnt/PCP signalling is activated during differentiation of ISCs towards PCs and EECs.

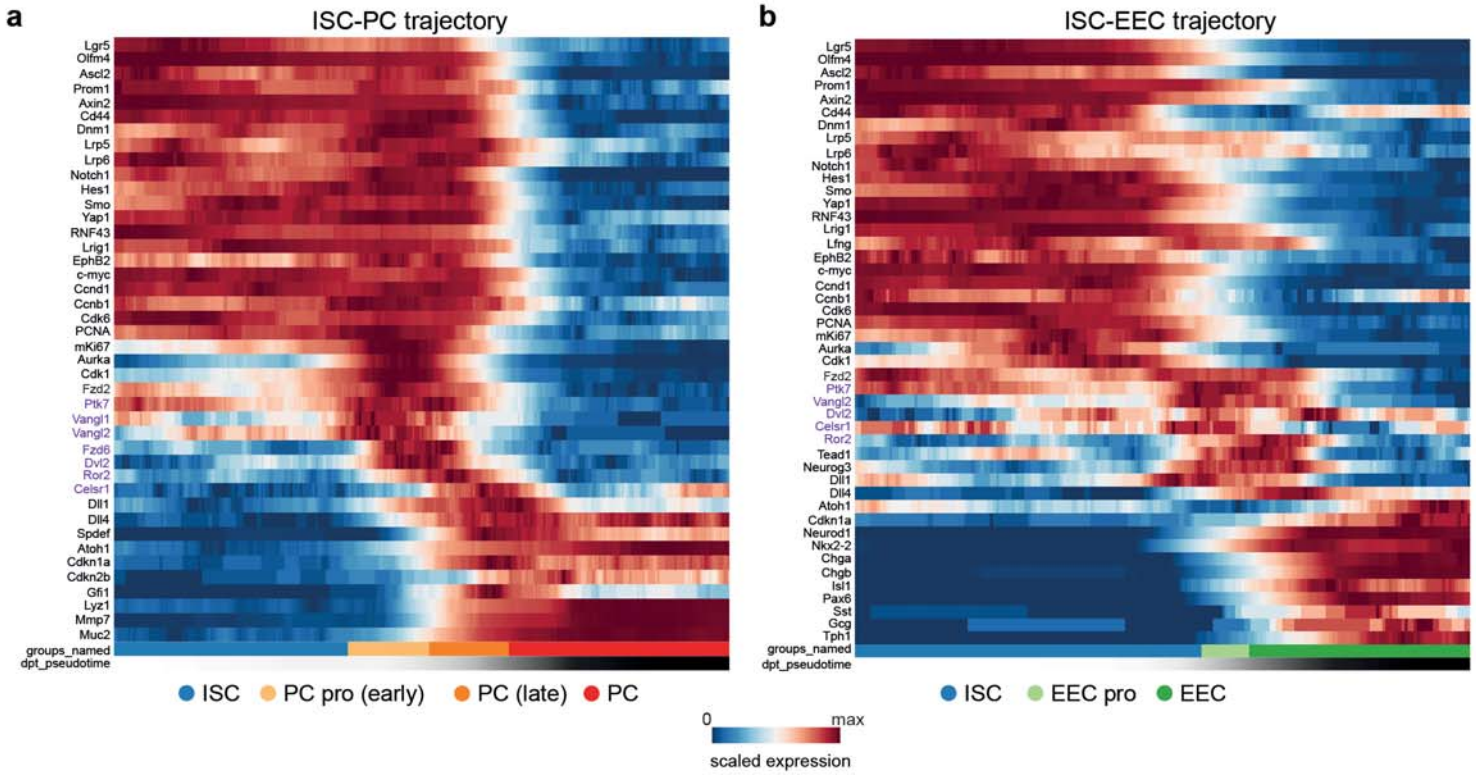

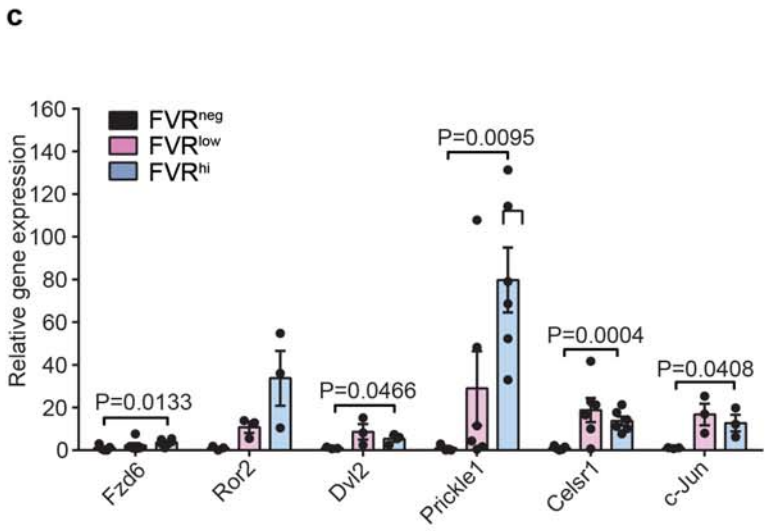

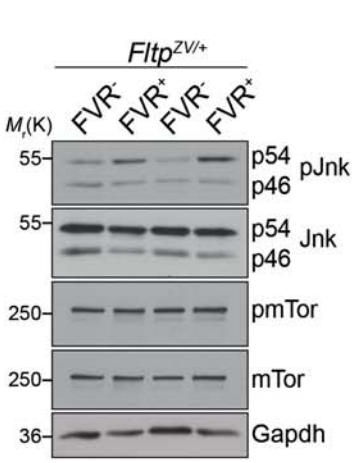

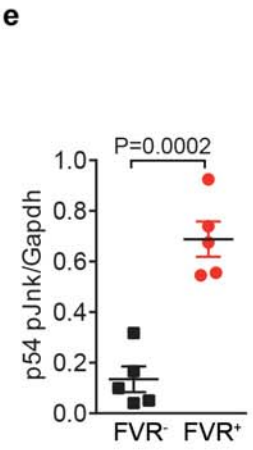

Böttcher et al. Extended Data Figure 8

Disturbed Wnt/PCP signalling causes alterations in gene expression pattern and numbers of Paneth cells.